Molecular dynamics of ionic solid and liquid surfaces

David M. Heyes
Department of Chemistry, Royal Holloway College, University of London, Egham, Surrey TW20 OEX, United Kingdom
(Received 26 July 1983)

Molecular-dynamics computer simulations of model alkali halide solids and melts were performed with the aim of elucidating the role of electrostatic interactions in the determination of bulk and interphasial behavior. Simplified pair potentials of the n:1 form are shown to compare favorably with the results of the more complicated Born-Mayer-Huggins potential, and have great corresponding states capability. New lattice-summation techniques for obtaining the long-range Coulomb correction are also discussed, which are markedly different from the usually adopted Ewald formulas. The properties of solid and liquid surface states were examined under the influence of vacuum and rigid-wall constraints. Both boundaries have noticeable effects on the material to a depth of 10—20 Å into the bulk of the material. Charge separation in the vacuum interphase of model molten LiCl was not observed. The problems associated with definitions of pressure and diffusion coefficients in the interphase are discussed and results are presented. Attempts were made to produce surfaces which would be polar under steady-state conditions. An applied electric field in the direction perpendicular to the surface plane for a melt/vacuum interface did not induce any observable charge separation. It was necessary to apply an electric field equivalent to four times the root-mean-square force at equilibrium before ion desorption into the adjacent vacuum was observed. This took the form of infrequent departures of ion pairs. Slow surface structural evolution was demonstrated by applying an electric field parallel to the surface. The interphasial ionic mobilities were *smaller* there than in the bulk. The highly polar (111) model NaCl solid surface was unstable with respect to an, as yet, undetermined reconstructed form.

I. INTRODUCTION

In recent years there has been much activity in the field of surface modeling. The thermodynamics and structure of plane and curved liquid-vapor interphases, consisting of molecules interacting with short-range forces, has received attention by Rowlinson and others.[1,2] In contrast, there has been a rather sporadic interest in surfaces consisting of charged species (except at extreme dilutions). In the dilute-concentration regime Torrie and Valleau[3] and Snook and van Megen[4] have used Monte Carlo simulation to demonstrate the success of the Gouy-Chapman theory in describing double-layer effects in model dilute electrolytes. The literature on integral-equation solutions to this system is also substantial and goes back to before the time of Debye and Hückel and the earliest theories of electrolyte solutions.[5–9]

In contrast it is only recently that the surface structure of molten salts has been seriously investigated,[10–12] because of problems associated with the high density of these systems and the need for a suitable reference state. Evans and Sluckin[10,11] have used a density-functional theory for inhomogeneous charged fluids, an approach which was in fact first proposed by van der Waals. Other work has shown that the structure of a liquid in the surface region is more ordered than in the bulk. Pair correlations near a hard wall[13] or in the interfacial electrical double layer[14,15] are long ranged. As in the bulk of a molten salt[16–24] the Coulomb interaction at short range dominates the ordering and tends to diminish the importance of the other short-range terms in the interionic potential (e.g., core repulsions, dispersion terms) when comparison with the appropriate noble-gas liquids is made.

The importance of the Coulomb interaction in determining the stability and hence structure of ionic crystal surfaces has been recognized for a long time.[25–31] Idealized crystal surfaces which exhibit a dipole moment in the direction perpendicular to the surface have been shown analytically to be unstable to rearrangement so that this dipole is nullified in a manner which takes little account of the short-range interactions between the ions.[25] Certainly the scant experimental evidence for such high-index crystallographic faces gives support for this assertion. A realization of the overriding influence of the Coulomb part of the interionic potential of alkali halides has impacted recently on a redesigning of these interactions in order to minimize the complexity of the short-range terms (especially for liquid-state investigations) in recognition of the importance of the Coulomb term. Notably, Woodcock[32,33] has attempted to replace the Born-Mayer-Huggins (BMH) interaction form for alkali halides by one characterized by the depth of the potential, ϵ, and the separation at its (gas-phase) minimum, r_0. Similar investigations into developing a corresponding-states treatment for alkali halides have been made,[34–36] but with little success.

The BMH pair potential between ions i and j, $\phi_{ij}(r)$, is

$$\phi_{ij}(r)=A_{ij}\exp(-br)+q_iq_jr^{-1}+C_{ij}r^{-6}+D_{ij}r^{-8}\,, \qquad (1)$$

where the parameters are those derived by Tosi and Fumi.[37] q_i is the charge on ion i and r is the distance be-

tween ions i and j. The first, second, third, and fourth terms represent the short-range repulsion, Coulomb, dipole-induced dipole, and dipole-induced quadrupole interactions, respectively. On a suggestion by L. V. Woodcock, a special case of a general $m:n$ potential,

$$\frac{\phi_{ij}(r)}{\epsilon}=\frac{m}{n-m}\left[\frac{r_0}{r}\right]^n\pm\frac{n}{n-m}\left[\frac{r_0}{r}\right]^m, \tag{2}$$

was considered as a simplification by taking $m=1$ and $n=12$, 10, 8, or 6. Note that in reduced units of $\phi^*_{ij}=\phi_{ij}/\epsilon$ and $r^*=r/r_0$, the potential always minimizes at $\phi^*_{ij}=1$ and $r^*=1$ for unlike species. On taking $m=1$, then

$$\phi^*=\frac{1}{n-1}(r^*)^{-n}\pm\frac{n}{n-1}(r^*)^{-1}. \tag{3}$$

For many salts $\epsilon^*/(e^2/4\pi\epsilon_0 r_0)$, where ϵ_0 is the permittivity of free space, ranges from 0.88 to 0.98. By choosing $n=12$ we ensure that the Coulomb-type term in Eq. (3) decays in a quantitatively similar fashion to the true Coulomb interaction. However, this is not necessarily the aim here.

Adams and McDonald[34] considered a similar potential,

$$\phi_{ij}(r)=\frac{e^2}{r_0}\left[\frac{1}{n}\left[\frac{r_0}{r}\right]^n-\left[\frac{r_0}{r}\right]\right]. \tag{4}$$

Here the unit of energy is fixed in order to give the true Coulomb decay at distant separations, i.e., e^2/r. It could be argued that this is a less satisfactory constraint because in a melt it is unrealistic to assume that molecules interact with a r^{-1} form when separated by a highly polarizable medium of ions. From a corresponding-states point of view it is also unsatisfactory, because the minimum in the potential is always $[(1-n)/n]e^2/r_0$ and hence is dependent only on r_0 (plus the choice of n). Consequently ϵ and r_0 are not independent in the model of Eq. (4), which makes it a very restrictive approach. This is an injudicious constraint because the long-range part of the potential need not decay as the Coulombic monopole-monopole interaction. In fact one might suspect this by the success of the Ewald complementary error-function expression (without most of the reciprocal-lattice component), which is often used to replace the Coulombic term and still gives excellent thermodynamic quantities for the infinite system.[33] It is more sensible to allow the minimum in the pair potential to be another variable which is independent of r_0. Polarization effects will affect the depth of the potential minimum. Providing these minima can be located by more complete computer simulation studies (including polarization terms) or by analysis of experimental gas-phase data, then it forms a more solid foundation for basing a corresponding-states treatment of alkali halide melts.

In the following section molecular-dynamics (MD) computer simulations of solid and liquid model alkali halides are considered. An overview of a number of bulk and interphasial simulations is made to provide new insights into the role of the Coulombic term in determining many aspects of ionic system behavior.

II. MODELS AND RESULTS

The MD model used for most of these calculations has been described elsewhere.[38,39] Bulk calculations described here were made with the usual periodic boundary conditions for systems of 216 ions confined within a cubic cell of sidelength S, and using the proven Ewald method to incorporate the long-range Coulomb interactions.[38] The time step was typically 0.75×10^{-14} s for the melt calculations. The surface calculations were performed by creating periodic images in only the x and y directions from the orthorhombic MD unit cell. Most of these used a modification of the Ewald method to obtain the long-range Coulomb corrections.[38]

In the later stages of this study another (more easily implemented) method was adopted.[40] The background to this real-space lattice-summation technique and its relationship to the Fourier-transform approaches (of which the Ewald method is an example) is now presented.

A. Lattice summations

Let ϕ_{ij} denote the Coulomb potential energy between two point charges q_i and q_j. As j forms a distinct sublattice it is implicit that all the images of the chosen origin j are included in this interaction. Let j_0 be this chosen charge which we will define as the origin of the coordinate system. This would correspond to the central ion of a reoriented MD cell. Hence,

$$\phi_{ij}=q_i\sum_j q_j r_{ij}^{-1}, \tag{5}$$

where the above summation is over j_0 and its images (unless $i=j_0$, in which case j_0 is omitted), and where $r_{ij}=|\vec{r}_i-\vec{r}_j|$ and $\vec{r}_i$ is the absolute position of charge i.

Equation (5) is a slow conditionally converging series, which means that the limit (i.e., ϕ_{ij}) depends on the order in which the component terms from the lattice are summed. Methods for obtaining the limit of a slowly converging series from a finite number of terms is a well-developed area of algebra.[41]

In the early stages of this work, a number of such methods for performing these lattice sums were investigated with the view of using them in molecular-dynamics simulations. At first it was thought that a recasting of Eq. (5) as a sum in reciprocal space[42–44] (an approach extensively used in static-lattice/lattice-dynamics studies) would be efficient. The potential at ion site i, Φ_i, is given by

$$\Phi_i=S_1^{-1}S_2^{-1}\sum_{\vec{h}}\sum_{j=1}^{N}q_j\exp(-2\pi i\vec{h}\cdot\vec{r}_{ij})\times\exp(-2\pi h\,|\,r_{zij}\,|\,)/h, \tag{6}$$

where $\vec{h}$ is a reciprocal-lattice vector of a two-dimensional sublattice and r_{zij} is the component of r_{ij} in the direction perpendicular to the sublattice planes.

This method was found to be unsuitable, however, because of the large number of reciprocal-lattice vectors which are required to represent the potential as the separation between the charges in the direction perpendicular to the sublattice planes approaches zero. Quite fundamentally, there is a different requirement in the static-

(regular-) lattice calculations which make variants of Eq. (6) acceptable methods. In a regular lattice the point charges are separated by zero or a large distance (i.e., $\approx$interionic spacing) in the z direction. Reciprocal-lattice formulas for the potential (and hence forces) are available under these limits, which usually only have to be evaluated once at the beginning of the calculation. In MD these sums need to be performed at regular intervals and the troublesome $r_{zij} \rightarrow 0$ region is frequently encountered. Therefore, the requirements of a lattice-summation scheme are more demanding for MD. In passing we note that these formulas do demonstrate (through the zero reciprocal space-vector component) the instability of a semi-infinite crystal with a unit-cell dipole moment which has a nonzero component perpendicular to the surface.

These special requirements for MD are better met using a method based, at least partially, on sums over the real lattice[45–47]—because truncation errors are less likely to introduce big changes in potential. For example, Woodcock and Singer[46] used the Ewald method to treat bulk ionic systems. This consists of a hybrid real-space—reciprocal-space expansion to evaluate the electrostatic potential at each ion site. This was developed by Heyes *et al.* to apply to the MD of ionic interfaces[38,39] and this approach is used for most of the calculations performed for this work. However, a technically simpler method which would be cast entirely in real space was also sought.

One can avoid performing the image lattice summations for each ij interaction by expanding the potential of the jth image lattice about its origin generator, j_0, using a Maclaurin's series expansion.[41] The effects of all the j images can then be expressed in terms of a polynomial containing the components of $\vec{r}_i$, which is the coordinate of ion i within the unit cell and measured with respect to the position of j_0 as the origin. The constants in this expansion are given in terms of lattice sums involving powers of $r_{jj_0}^{-1}$.[48] Unfortunately agreement with the exact result was poorest for large $\vec{r}_i$, which extend into the corners of the unit cell. Here the contributions to the forces from the lattice outside the unit cell are a significant proportion of the total force. This is perhaps to be expected as a natural property of a Maclaurin's series expansion and which causes a failure in this approach.

A related method, involving an expansion of the unit cell in multipoles, was also investigated.[49] A lattice of dipoles, quadrupoles, and octupoles was established. The potential and forces due to this system were compared with the exact results for a test MD cell configuration chosen at random. The contributions to the potential from each replica square-shaped shell of MD cells beyond the fourth is well given by the quadrupolar term in the multipole potential expansion. However, as the shells closer to the origin MD cell are approached, higher multipoles are needed to such an extent that the method becomes uncompetitive when compared with the Ewald-type method already developed. A similar trend is noted for the multipole forces as well.

Finally, perhaps the simplest method for evaluating the lattice sum potential was investigated. This is by adding the r^{-1} terms of Eq. (5) in a new specified order. The Evjen method was dismissed by earlier workers in the field of MD simulations of dense ionic media[46] because it led to distorted, unphysical structures. At the time, it was thought that not enough image shells were taken. However, in fact, it has recently been shown that only one image shell of square symmetry is needed to give a good representation of the potential provided certain correction terms to transform from the so-called extrinsic to intrinsic potential are included.[40] As Eq. (5) is conditionally convergent, the order in which the image j are included in the sum is important. For a two-dimensional periodic charge distribution it is proposed to sum the image j in "circular" shells. This is adopted because it then becomes easy to define the effect, at long range, from an ever increasingly wider and more truly circular annulus of MD cells about the origin. This correction (or "depolarization") potential has been discussed elsewhere by the author for static systems,[40,50,51] without specific reference to MD. For two-dimensional periodicity then

$$q_i^{-1}q_j^{-1}\phi_{ij} = \lim_{R_c\rightarrow\infty}\left[\left(\sum_j r_{ij}^{-1}\right) + \frac{\pi}{2S_1S_2R_c}(r_{xi}^2 + r_{yi}^2 - 2r_{zi}^2)\right], \quad (7)$$

where R_c is the radius of the circle of MD images and $r_{ij} \leq R_c$. Hence,

$$q_i^{-1}q_j^{-1}F_{xi} = \lim_{R_c\rightarrow\infty}\left[\sum_j r_{xij}r_{ij}^{-3} - \frac{\pi r_{xi}}{S_1S_2R_c}\right] \quad (8)$$

and

$$q_i^{-1}q_j^{-1}F_{zi} = \lim_{R_c\rightarrow\infty}\left[\sum_j r_{zij}r_{ij}^{-3} + \frac{2\pi}{S_1S_2R_c}r_{zi}\right]. \quad (9)$$

The convergence characteristics of the Evjen, depolarized Evjen [Eqs. (7) to (9)], and surface Ewald methods are compared in Table I, for a square planar lattice of unit-cell sidelength S.

The depolarized Evjen (DE) method gives very satisfactory values for the potential and force if the nearest square shell of (8) image cells are included in the expansion. Errors in the potential of less than $0.05S^{-1}$ are typical for the test configurations. The Evjen method produces errors an order of magnitude larger (i.e., $\sim 10k_BT$) and it is perhaps not surprising that this method gives noticeably distorted structures. The DE method showed sufficient promise in these trial calculations to have warranted incorporation in an MD program. Test simulations on a 216 ion ($6\times6\times6$) MD double-vacuum interface simulation took 0.14 on the University of London Computer Center Cray-1S, which compares favorably with MDIONS,[52] a similar Ewald program. Root-mean-square total energy fluctuations for the system run at "constant energy" were 0.003 kJ mol^{-1} for room-temperature model KCl (using Tosi-Fumi parameters in the BMH rigid ion potential) and 0.02 kJ mol^{-1} for molten NaCl near its triple point.

TABLE I. The potential at a point $\vec{r}=0$ due to two square planar sublattices: $q_1=q$ at (x_1,y_1,z_1) and $q_2=-q$ at (x_2,y_2,z_2). Φ is in units of qS^{-1}. The x component of the force, F_x, and F_z, the z component of the force, are in units of qS^{-2}. E_w—Ewald-type expansion (Refs. 40 and 50); E—Evjen summation (Ref. 51); DE—depolarized Evjen from Eqs. (7)–(9). $R_c=(\underline{l}^2S^{-2}+1)^{1/2}S$ in these expressions where $\underline{l}$ is the integer index of the image cell's displacement in the unit of S (see Ref. 40). $n=1$, $\eta=0.7S$ in E_w; (x_1,y_1,z_1) and (x_2,y_2,z_2) are $-(0.25,0.15,0.20)S$ and $-(0.40,0.32,0.20)S$, respectively. $n=2$, $\eta=0.7S$ and $-(0.499,0.15,0.10)S$ and $-(0.40,0.32,0.40)$. $n=3$, $\eta=0.7S$ and $-(0.25,0.15,0.10)$ and $-(0.40,0.32,0.40)$. $n=4$, $\eta=0.7S$ and $(0.499,-0.15,-0.10)$ and $-(0.1,0.32,1.0)$. $n=5$, $\eta=0.7S$ and $-(0.1,0.2,0.1)$ and $-(0.15,0.1,0.15)$.

n	$\underline{l}^2S^{-2}$	Φ (E_w)	Φ (E)	Φ (DE)	F_x (E_w)	F_x (E)	F_x (DE)	F_z (E_w)	F_z (E)	F_z (DE)
1	0	0.8589	1.0099	0.7313	3.3938	3.2515	3.7227	3.2525	3.3228	3.3228
1	1	0.7555	0.9513	0.7542	3.4744	3.1535	3.4867	3.0738	3.1365	3.1365
1	2	0.7098	0.8671	0.7062	3.6378	3.3683	3.6403	3.0154	3.0460	3.0460
1	64	0.7090	0.7442	0.7096	3.6417	3.5821	3.6405	3.0146	3.0150	3.0150
1	900	0.7090	0.7183	0.7090	3.6417	3.6260	3.6417	3.0146	3.0146	3.0146
2	0	0.9622	0.3461	0.8317	1.6365	1.8840	1.5730	−3.0523	−0.7875	−2.6725
2	1	1.3214	0.9259	1.2693	−0.3942	−0.1491	−0.3690	−3.1096	−1.5912	−2.9241
2	2	1.3280	1.0320	1.3123	−0.3881	−0.1306	−0.3102	−3.1898	−2.0818	−3.1700
2	64	1.3290	1.2675	1.3278	−0.3971	−0.3571	−0.3957	−3.1906	−2.9521	−3.1859
2	900	1.3290	1.3128	1.3290	−0.3971	−0.3867	−0.3970	−3.1906	−3.1277	−3.1905
3	0	2.1582	1.7058	1.8984	7.1290	7.0809	7.5522	−0.3450	1.9581	0.0732
3	1	2.1930	1.9970	2.1332	6.8889	6.6581	6.9913	−0.7702	0.7790	−0.5538
3	2	2.1696	2.0451	2.1563	6.9676	6.7457	7.0177	−0.8685	0.2569	−0.8314
3	64	2.1691	2.1447	2.1686	6.9699	6.9108	6.9693	−0.8701	−0.6314	−0.8652
3	900	2.1691	2.1627	2.1691	6.9699	6.9542	6.9699	−0.8701	−0.8071	−0.8699
4	0	4.3047	0.9366	4.2967	−2.5746	−3.4263	−1.5445	−4.6703	−0.1828	−5.8377
4	1	4.8714	2.4741	4.8500	−0.2086	−1.3573	−0.0266	−4.2242	−0.7793	−4.7779
4	2	4.9237	3.0763	5.0163	−0.0507	−1.0996	−0.0132	−4.2037	−1.3899	−4.6547
4	64	4.9256	4.5022	4.9190	−0.0373	−0.2744	−0.0410	−4.2030	−3.4941	−4.1955
4	900	4.9256	4.8135	4.9255	−0.0373	−0.1001	−0.0374	−4.2030	−4.0144	−4.2027
5	0	−0.1138	−0.1815	−0.1148	−4.7212	−4.8250	−4.6679	−5.2115	−4.8250	−5.1392
5	1	−0.0871	−0.1379	−0.0907	−4.5589	−4.6624	−4.5513	−5.2507	−5.0059	−5.2280
5	2	−0.0841	−0.1226	−0.0841	−4.5563	−4.6461	−4.5554	−5.2531	−5.0737	−5.2551
5	64	−0.0841	−0.0925	−0.0842	−4.5559	−4.5757	−4.5563	−5.2531	−5.2134	−5.2524
5	900	−0.0841	−0.0863	−0.0841	−4.5559	−4.5612	−4.5559	−5.2531	−5.2426	−5.2531

B. Short-range potential

The choice of the short-range components of the potential is now discussed. In the Introduction, it was suggested that the structure of a melt could be reproduced by a simple n:1 potential as given in Eq. (3). Test bulk calculations on a model KCl melt at 1045 K and a molar volume, $V_m=51.24\ \mu m^3 mol^{-1}$, were performed for n ranging from 8 to 12, although only the behavior of the two extremes is explicitly discussed here. The Ewald potential with $\eta=0.175S$ was used.[51] This is a well-characterized state[39] with a total energy per particle of $-625\ kJ\,mol^{-1}$ and pressure of 0.8 kbar using the BMH potential.

The structure of each melt was examined in terms of the partial pair radial distribution functions, $g_{ij}(r)$, for species i and j,

$$g_{ij}(r)=Vn_{ij}(r)/N\,dV_{ij}(r)\ , \tag{10}$$

where V is the volume of the MD cell ($=4S^3/3$), N is the number of ion pairs in the cell, and $n_{ij}(r)$ is the average number of ions of species j in a radial volume element between $r-dr/2$ and $r+dr/2$ around a particular ion of type i. The volume element is $dV_{ij}(r)=4\pi r^2dr$ and $dr=0.1$ Å here.

Figure 1 shows the computer-generated pair radial distribution functions of the bulk liquid simulations. The 1045-K KCl BMH $g_{ij}(r)$ at $V_m=51.24\ \mu m^3 mol^{-1}$ are compared with those of another work at $V_m=48.8\ \mu m^3 mol^{-1}$ and reveal a quite remarkable density insensitivity. The long-range order in KCl damps out more rapidly as distance increases at 1273 K than at 1045 K. A pair potential proposed by Michielsen *et al.*[53] produced slightly distinguishable cation-cation and anion-anion distribution functions, unlike those generated by the Tosi-Fumi (TF) KCl pair potentials at the same temperature and density.

Insights into the structural distortions caused by the ordinary Evjen method can be gained from the $g_{ij}(r)$ of a bulk simulation with $\eta=0.833S$ and truncating all in-

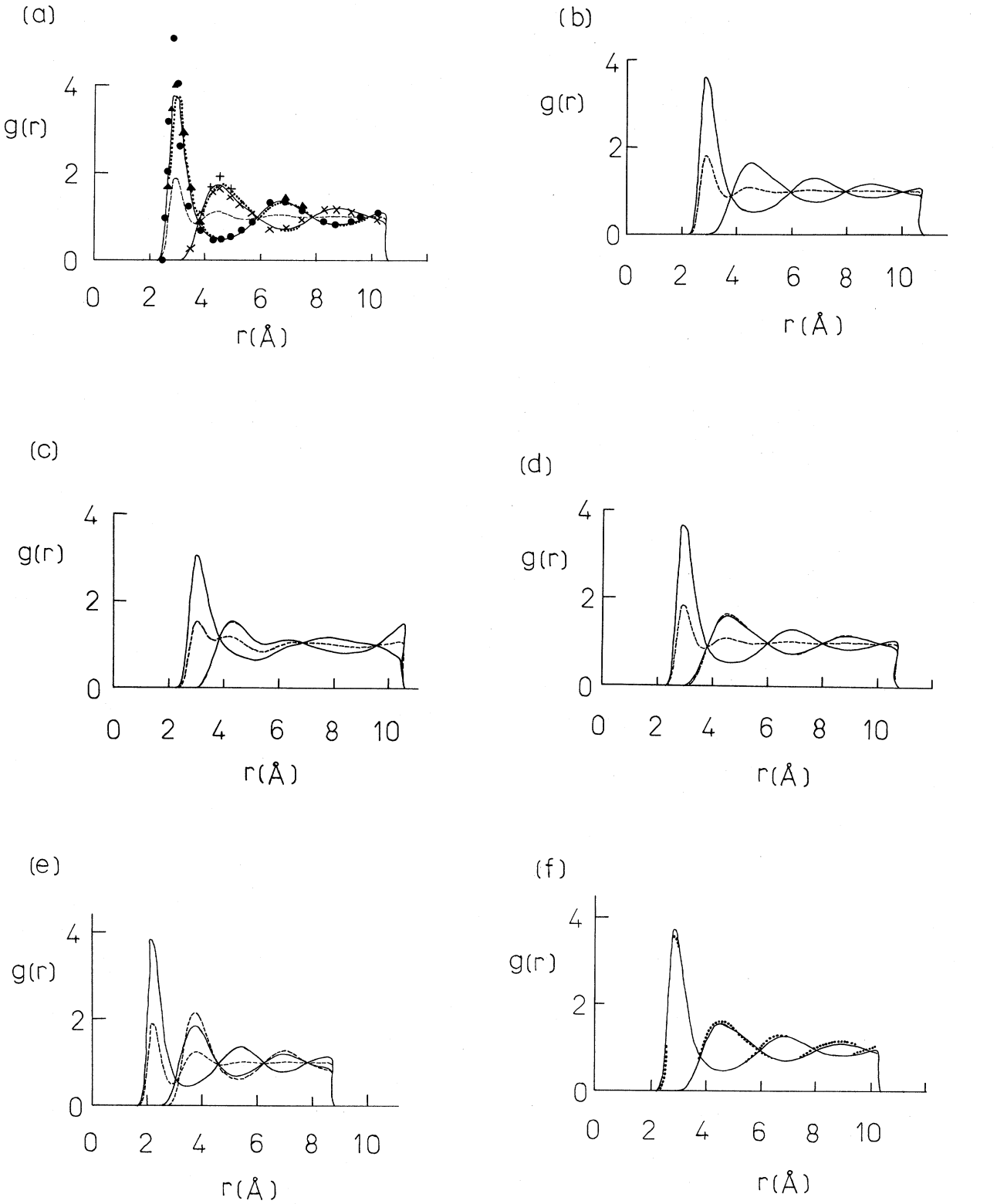

FIG. 1. Pair radial distribution functions, $g_{ij}(r)$, for species i and j; + for cation and − for anion. ——, g_{+-} or g_{++}; − − −, g_{--} or $\frac{1}{2}[\frac{1}{2}(g_{++}+g_{--})+g_{+-}]$. (a) Bulk TF KCl, $T=1045$ K and $V_m=51.24\ \mu m^3\,mol^{-1}$, · · · · other Monte Carlo TF work (Ref. 54) at $T=1043$ K and $V_m=48.80\ \mu m^3\,mol^{-1}$, $\eta=S/5.714$,●,×(12:1), and ▲, + (8:1) potential simulations. (b) Bulk TF KCl, $T=1273$ K and $V_m=54.00\ \mu m^3\,mol^{-1}$. (c) Bulk TF KCl, $T=1045$ K, $V_m=51.24\ \mu m^3\,mol^{-1}$, $\eta=S/1.2$ (truncation at $S/2$). (d) Bulk Michielsen KCl, $T=1273$ K, $V_m=54.00\ \mu m^3\,mol^{-1}$. (e) Bulk TF LiCl, $T=883$ K and $V_m=29.10\ \mu m^3\,mol^{-1}$. (f) · · · · Bulk TF KCl, $T=1273$ K and $V_m=54.00\ \mu m^3\,mol^{-1}$, —— directionally indiscriminate pair radial distribution functions in the center of the corresponding liquid film with two vacuum-melt surfaces.

teractions beyond $S/2$. The potential jump at this truncation is $\sim 6k_BT$. This produces (as would the r^{-1} Coulomb interaction) a distorted structure in which unlike ions seek relative positions within the cutoff radius and like ions accumulate beyond this distance.

Also in Fig. 1 the $g_{ij}(r)$ of a 833-K model LiCl TF simulation are shown. Although there is a greater penetration into the first coordination shell of like ions for Li^+ than Cl^- (due probably to ion size differences) the like-ion first peaks coincide. Charge ordering is substantial and diminishes the importance of the short-range components of the potential. The LiCl bulk simulation had a total energy and pressure of -780.2 kJ mol^{-1} and 0.32 kbar. These agree well with Monte Carlo predictions of -781.1 and ~ 0.0 obtained elsewhere for the same pair potential.[55]

Pair potentials which were simpler than the BMH potential were also considered in this exploratory stage. Some test MD simulations for the equivalent KCl state at $T=1045$ K and $V_m=51.24$ μm^3 mol^{-1} using the Woodcock potential of Eq. (3) were performed. To convert from real to $(n:1)$ units we use the following relationships: for the reduced number density, ρ^* $(=Nr_0^3/V)$, reduced temperature, T^* $(=k_BT/\epsilon$, where k_B is Boltzmann's constant), reduced time step, Δt^* $(=\Delta t\,\epsilon^{1/2}/\sigma m^{1/2}$, where m is the mass of both species), reduced internal energy, u^* $(=u/\epsilon)$, and reduced pressure, P^* $(=P\sigma^3\epsilon^{-1})$:

$$\rho^* = 1.204\,504(r_0/\text{Å})^3 V_m^{-1} ,$$

$$T^* = 5.984\,47\times 10^{-6}(T/\text{K})(r_0/\text{Å})(\epsilon^*)^{-1} ,$$

$$\Delta t^* = 372.735\,34(\Delta t/\text{ps})\epsilon^*(m/\text{amu})^{-1/2} \times (r_0/\text{Å})^{-3/2} ,$$

$$u^* = 3.5985\times 10^{-4}(u/\text{kJ mol}^{-1})(r_0/\text{Å})(\epsilon^*)^{-1} ,$$

$$P^* = 0.433\,44\times 10^{-4}(P/\text{kbar})(r_0/\text{Å})^4(\epsilon^*)^{-1} .$$

For model KCl at $T=1045$ K and $V_m=51.24$ μm^3 mol^{-1}, then $\rho^*=0.4457$ and $T^*=0.017\,67$. Here $\epsilon=7.785\times 10^{-19}$ J, i.e., $\epsilon^*=0.90$ if $r_0=2.6666$ Å.[33] It is noteworthy that the reduced temperature at the triple point is approximately $\frac{1}{50}$ of the well depth [in marked contrast to the corresponding Lennard-Jones (LJ) liquid[52] in which $T^*\approx 0.72$]. One considers melts to be "high-temperature" liquids, but in fact they form at quite low (internally standardized) temperatures. The deep potential well is the result of very strong Coulomb "point-charge" interactions. Consequently the structure of an ionic melt is more likely to be determined by a much narrower portion of the pair potential than that of the LJ liquid, primarily at the base of the potential bowl.

The Tosi-Fumi BMH liquid under these conditions has a total (including kinetic) energy and pressure of -624.8 kJ mol^{-1} and 0.8 kbar, respectively. The n:1 fluids of Eq. (3) for $n=12$, 10, and 8 give for the total energy -640.4, -628.9, and -608.1 kJ mol^{-1}, respectively. The corresponding pressures are -1.6, 1.5, and 9.0. The 10:1 example gives reasonable agreement with the Tosi-Fumi thermodynamic properties but structurally the best correspondence is achieved using the 8:1 potential. The first unlike-ion peak in the pair radial distribution function for $n=12$, 10, and 8 has a height of 5.2, 4.4, and 4.0, respectively. The Tosi-Fumi value is 3.8. The sharpening of this peak follows from a corresponding narrowing of the potential bowl which is illustrated in Fig. 2. Except for the fine details of this peak, all other features are rather insensitive to the choice of n and give good agreement with those generated by the more complicated Tosi-Fumi BMH potential. Thus it is to be concluded that these simple pair potentials have some promising properties in reproducing many features of melt behavior, when based solely on a number of simple independent (but significantly *measurable*) parameters such as the minimum in the pair potential. It is worth noting that the choice of n does have some bearing on "finetuning" the state of the modeled system to achieve conformity with the Tosi-Fumi state. Consequently, ϵ and r_0 are perhaps not the only parameters needed. It is relevant in this context that experimental data have a probable error of $\pm 5\%$, which is the variation between $n=12$ to 8. A value of $n=8.28$ for the related Pauling potential[34] is satisfyingly close to the optimum value empirically discovered here.

The KCl crystal at the melting temperature was simulated using the 12:1 potential. The first peak had a height of 4.1, which is quite close to the BMH prediction of 3.9

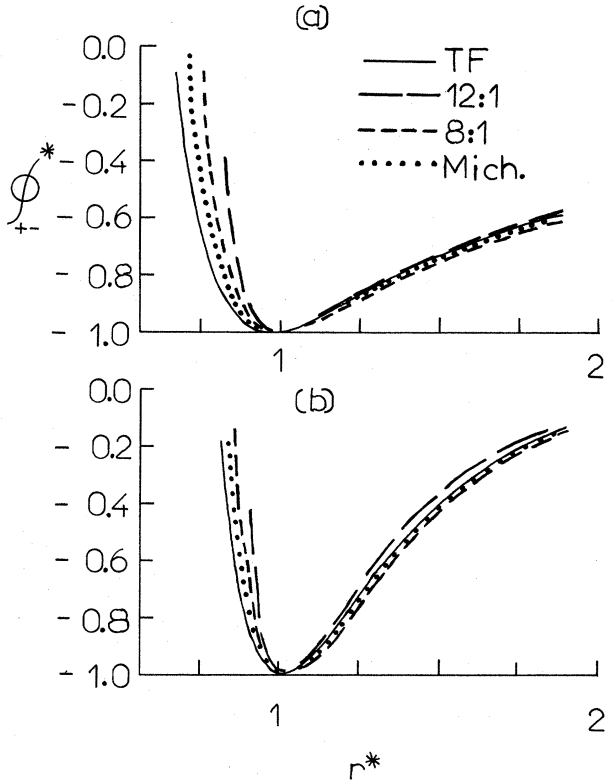

FIG. 2. KCl unlike-ion pair potentials $\phi_{+-}(r)/\epsilon=\phi^*_{+-}(r)$. $\epsilon=7.785\times 10^{-19}$ J (TF), $r^*=r$ (Å)/2.6666. (a) —— Tosi-Fumi BMH Eq. (1); — — — Eq. (3), $n=12$; - - - Eq. (3), $n=8$; · · · · Michielsen potential (Ref. 53). (b) As for (a) except that r^{-1} is replaced by $\text{erfc}(r/\eta)r^{-1}$ where $\eta=S/5.714$ and $S=20.945$ Å.

for the state $V_m=41.48\ \mu m^3 mol^{-1}$ ($\rho^*=0.550\,61$) and $T=1015$ K (or $T^*=0.017\,67$). As the ions do not approach one another so closely in the solid it is perhaps not surprising that the details of the short-range component of the potential (i.e., the choice of n) should be less of a factor in determining the structural behavior of the solid than the liquid. Nevertheless the BMH u and P are -655.0 kJ mol^{-1} and 21.2 kbars. The corresponding 12:1 values are -661.2 kJ mol^{-1} and -5.4 kbars; again this reflects the tensile or contractive pressure developed in a 12:1 material.

Often when the Ewald method is used to obtain the Coulomb interactions the Fourier-space component is omitted. The r^{-1} term in the pair potential is then multiplied by a complementary error function to produce a new, effective pair potential. The n:1 is in fact never used.[56] The shape of this effective potential is given in Fig. 2 and is shown to be quite different to that of the uneroded n:1 function.

The self-diffusion coefficients,[24] D, of these simple fluids were determined. The TF and 10:1 1045-K D values were 0.7×10^{-4} cm^2 s^{-1}. There was some evidence that the 8:1 and 12:1 self-diffusion coefficients are about 25% smaller but they had large statistical uncertainties. Attempts were made to "improve" the shape of the unlike-ion potential bowl, with the aim of reducing the height of the first peak in the pair radial distribution function. The point of inflection [i.e., $d^2\phi(r)/dr^2=0$] was fixed at $r^*=1.2$ but it produced little improvement.

It is perhaps worth clarifying the more important conclusions to be derived from the work described so far. The dominating role of the Coulomb term of the alkali halide potential in determining the gross features of melt structure in the bulk phase is evident. This permits a major simplification in the short-range potential when compared with the Born-Mayer-Huggins form. The derived thermodynamic properties are also not too sensitive to its shape *provided* that the well depth and position of the minimum separation are independent parameters, which should be obtainable from experiment or by more rigorous computer-simulation studies incorporating many-body polarization terms.

C. Interfaces

We now turn to consider the results of MD simulation of BMH crystalline and liquid films. Industrially molten salts are used frequently in applications which rely heavily on boundary-layer behavior.[57] Consequently a characterization of these states by MD modeling is a worthwhile aim. The solid and liquid films were simulated by replicating a MD cell of square cross section and sidelength S in the x and y directions only. Ions which passed through a face between the real and an image cell were returned through the opposite wall with the same wall coordinates and velocity. The long-range Coulomb corrections were evaluated as before,[38,39] except where stated when Eqs. (7) to (9) were used. The BMH bulk melt configurations described earlier were used to start the melt films.

The early simulations for solid and liquid coupled one surface of the film to an immobile boundary. In the case of the crystal this was a static ionic semi-infinite lattice whereas in the liquid it was a smooth wall with an attractive potential component to hold the film against it.

In order to assess the effects of the boundary changes we use the single-particle number density profile in the z direction which is defined to be perpendicular to any plane parallel to the surfaces,

$$\rho_i(z)=Vn_i(z)/N\,dV_i\ , \tag{11}$$

where $n_i(z)$ is the average number of ions of species i between the two xy planes at $z\pm\frac{1}{2}dz$, $dV_i=S^2dz$ is the volume element, dz equals 0.2 Å here. Before considering this function for the surface simulations we present the same function for a bulk MD cell (KCl, $V_m=54$ cm^3 mol^{-1}, $T=1273$ K) in Fig. 3. Both a species-resolved and an average ("indiscriminate") density profile are shown. There is no obvious correlation between fluctuations in the species-resolved profiles.

In Fig. 4 the $\rho_i(z)$ for an 8-layer model KCl (100) faced film, which was simulated at room temperature, is shown. There are 36 ions per layer within the MD cell. One face of the lamina is anchored to a semi-infinite fixed crystal of otherwise identical parameters. There is obviously a noticeable mismatch between the mobile and immobile crystal which is manifest in a sharpening of the peaks in $\rho(z)$ near the boundary between them. This is symptomatic of a lack of momentum transfer across the gap. The constrained and free surfaces have quite different dynami-

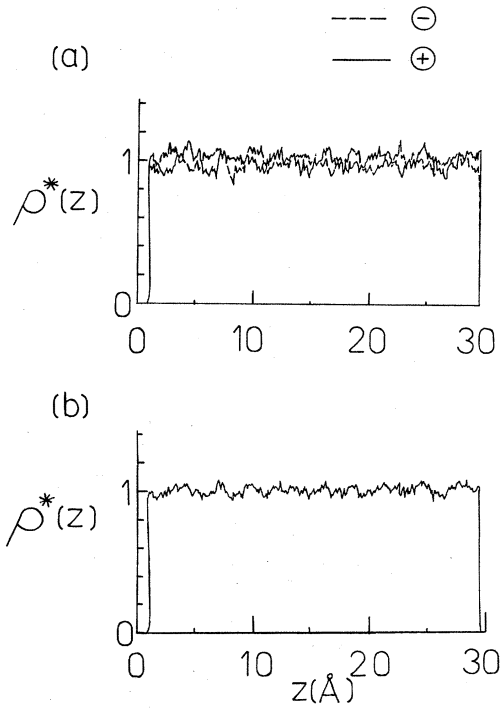

FIG. 3. (a) The reduced number density $\rho^*(z)=\rho(z)/\langle\rho\rangle$ for cation —— and anion — — — in a bulk model KCl simulation. $\Delta t=5\times10^{-15}$ s, $S=21.31$ Å, $T=1273$ K, $V_m=54.00$ μm^3 mol^{-1} and the number of time steps is 14 051. (b) As for (a) except that the average density for cation and anion is taken, i.e., $\frac{1}{2}[\rho^*_+(z)+\rho^*_-(z)]$.

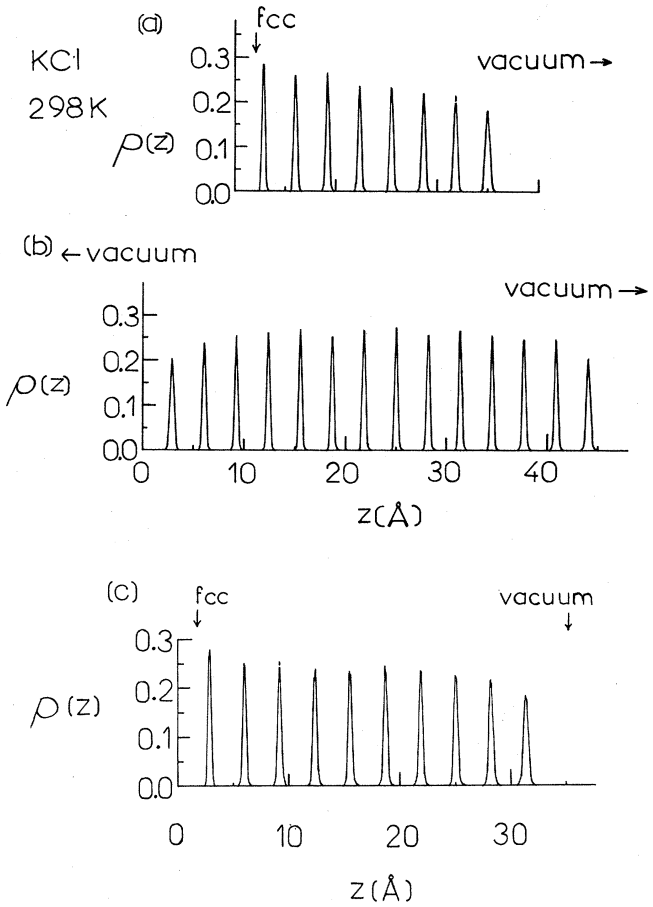

FIG. 4. (a) The density profile $\rho(z)$ of a 288-ion MD cell film coupled to a fixed semi-infinite lattice; $\rho(z)$ is normalized to unity for a regular crystal. $S=19.02$ Å; there are 36 ions per layer within the MD cell; the production simulation for this figure lasted for 5000 time steps of $\Delta t=5\times10^{-15}$ s. The left surface is coupled to the fixed crystal. The anion and cation components are denoted by — — — and ——, respectively. (b) As for (a) except that a 14-layer isolated film is considered. (c) As for (a) except that a 10-layer sample is considered.

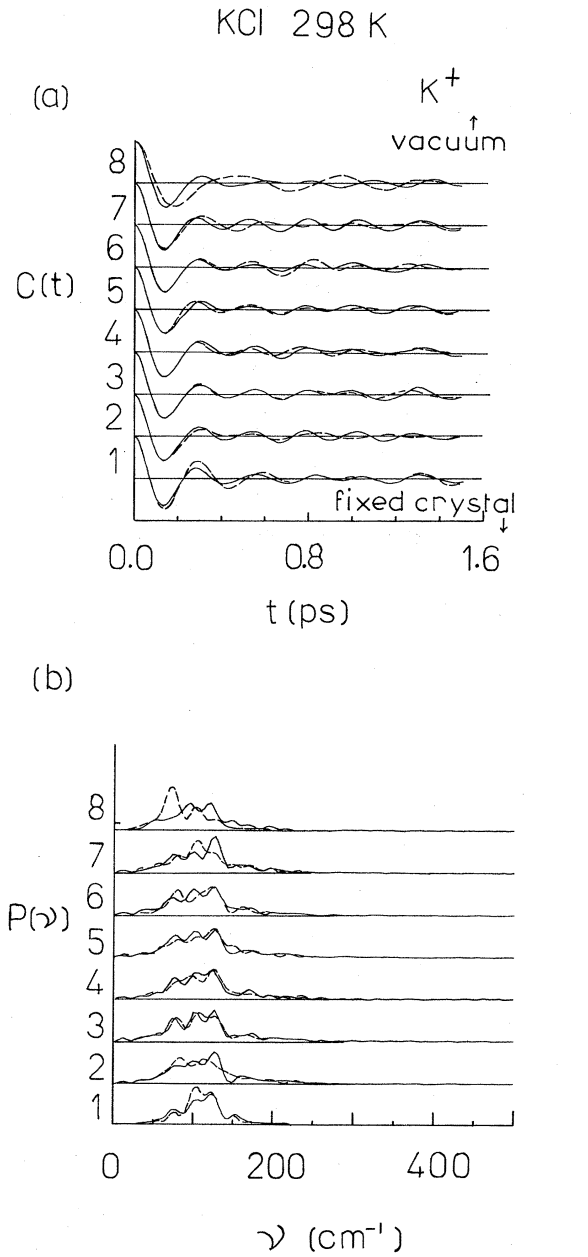

FIG. 5. A layerwise resolution of the (a) K^+ velocity autocorrelation function and (b) derived power spectra for the 8-layer system of Fig. 4. —— parallel to the surface, — — — perpendicular to the surface. 111 time origins were taken. Layer index, λ, equal to 1 corresponds to the layer next to the fixed crystal. Layer 8 is adjacent to a semi-infinite vacuum half space.

cal properties. A layerwise resolution of the velocity autocorrelation function[38] (VACF) in Fig. 5 in the directions parallel and perpendicular to the surfaces reveals that the layer next to the fixed crystal has a VACF similar but with noticeable differences to those in the center ("bulk") of the lamina. The free-surface layer shows, in contrast, damped motion in the perpendicular direction (effects which are perhaps better appreciated in the accompanying power spectra in Fig. 5). Figure 6 reveals that a 10-layer slab also manifests these effects and consequently they are not an artifact of the number of layers.

At first a smooth repulsive wall with an attractive tail was used for the liquid films. Figure 7 shows a 288-ion film (KCl) at 1273 K coupled to a wall potential with a depth of $-43k_BT$, $-24k_BT$, and $-5k_BT$ at $z=0.5$, 1.5, and 3.0 Å, respectively. This is a potential which is similar in shape and magnitude to the unlike-ion pair potential. The sharp density increase near the impenetrable hard boundary dies away rapidly so that by ~10 Å from the wall a region of uniform density is evident, which we can tentatively label "bulk" material. Also shown in Fig. 7 are the normalized velocity autocorrelation functions for the ions close to this wall. The component perpendicular to the wall is highly oscillatory. The perturbing effect of the wall is therefore to confine ions in the vicinity to a "latticelike" behavior. Later we will consider the use of

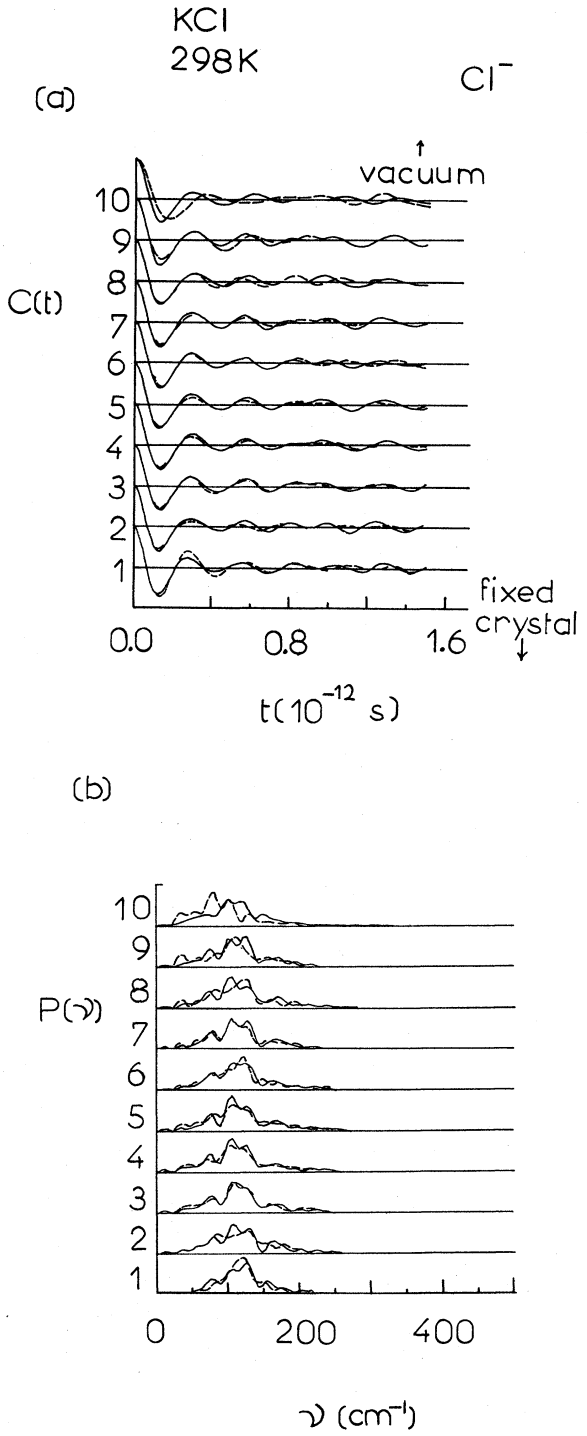

FIG. 6. As for Fig. 5 except that a 10-layer lamina is considered and the Cl^- dynamics are monitored.

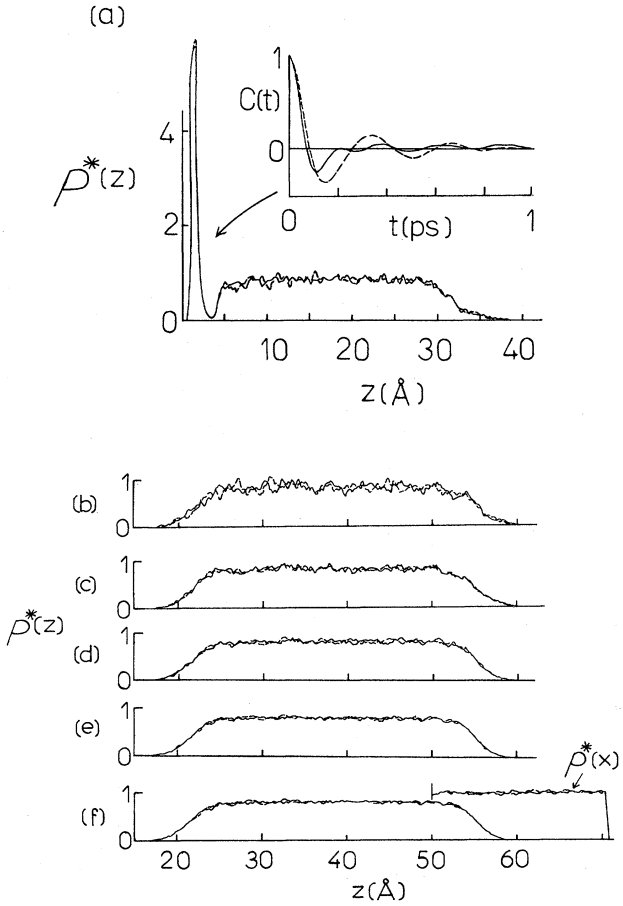

FIG. 7. The normalized accumulated single-particle density profiles, $\rho^*(z)$, of KCl model liquid films generated from a parent bulk configuration at $T=1273$ K and $V_m=54$ $\mu m^3 mol^{-1}$. $\rho^*(z)=\rho(z)/\rho$ (parent bulk). (a) Left surface coupled to an attractive smooth wall as described in the text ($t_{sim}=22.5$ ps). Two vacuum-melt interfaces at $T=1294$ K: (b) 16 ps, (c) 32 ps, (d) 68 ps, (e) 110 ps, (f) 152 ps. The insert is $\rho^*(x)$ for $t=147$ ps. The insert in Fig. (a) is the velocity autocorrelation function for K^+ parallel (——) and perpendicular (— — —) to the wall for those ions within $0 \lesssim z/Å \lesssim 10$.

such wall boundaries as a precursor to electrode modeling. For the present, however, we are only concerned with them in the ancillary role as an adjunct for obtaining melt-vacuum interfacial properties.

An alternative arrangement is to have two melt-vacuum boundaries as for the solid considered previously.[38] An example for a 1294-K KCl melt film is shown in Fig. 7 at selected stages in the simulation. Similar density profiles for model molten LiCl at 947 K are given in Fig. 8. An examination of the tangential and perpendicular VACF is also made in Fig. 8 for the ions in the central and surface regions. The cation and anion in LiCl are physically quite different species. Their radius and mass ratios are of order 0.54 and 0.2, respectively. This causes a highly structured VACF for Li^+ but a slowly decaying (rather featureless) Cl^- VACF. For both species, however, motion perpendicular to the surface is more unhindered in the surface region. This shows in the more damped VACF in the interphase. The power spectra of the surface perpendicular VACF maximize at ~ 40 cm^{-1} for Cl^- but ~ 230 cm^{-1} for Li^+.

The tangential, perpendicular (surface), and bulk diffusion coefficients (in 10^{-4} $cm^2 s^{-1}$) obtained from the mean-square displacements were 1.2, 1.2, and 0.96 for Li^+

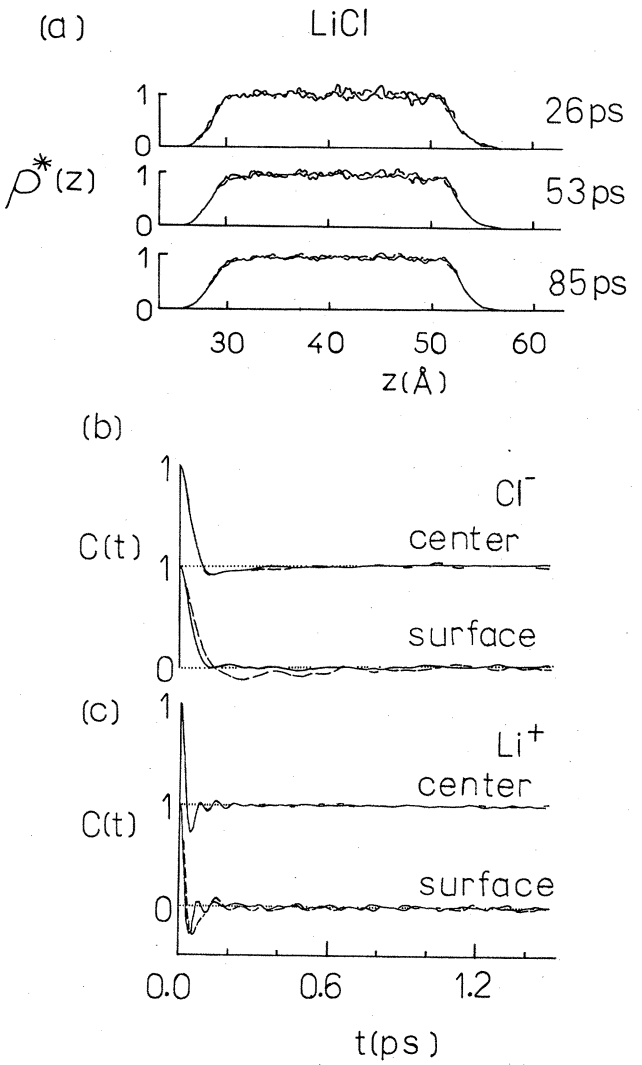

FIG. 8. (a) The accumulated normalized density profiles, $\rho^*(z)$, of a LiCl melt-free film simulation at 947 K at various times since the start of the simulation, which are denoted beside each profile. —— Li^+ and — — — Cl^- $N=288$. (b) The Cl^- velocity autocorrelation functions in the directions parallel (——) and perpendicular (— — —) to the vacuum-melt surfaces for the central ~35 and surface ~4 Cl^- ions. (c) As for (b) except that the Li^+ are considered.

and 1.1, 1.1, and 0.69 for Cl^-. These indicate an increased rate of diffusion in the interphase (perhaps inversely proportional to density[12]), which is common to all of the salts.

To conclude, there appear to be no obvious advantages in coupling a mobile film to a rigid boundary as a route to surface/vacuum behavior at the opposite interface. It is practicable to obtain two well-differentiated melt-vacuum surfaces with *less* computer time and still generate a bulk-like reference fluid in the middle of the intervening material.

The 1049 and 1294-K model KCl and 947 model LiCl "isolated" film calculations were performed using periodicity lengths in the x and y directions which are compatible with bulk simulations of 46.1, 48.6, and 29.1 $cm^3\,mol^{-1}$, respectively. As the parent bulk liquids had V_m of 51.24, 54.0, and 29.1 $cm^3\,mol^{-1}$, expansions of up to approximately 10% were therefore observed. A number of tests were performed to discover if these density decreases could be explained by slow equilibration. Density changes were suddenly imposed on test KCl films. The relaxation times for the response were less than 20 ps, which is approximately a fifth of the total simulation time for the above states. One should conclude that a density decrease for small systems is a thermodynamically established effect. In fact, this is a frequently observed phenomenon also in LJ films[58] and droplets.[1] A decrease in density of several percent is noticed when the thickness or diameter of the sample is less than approximately ten molecular diameters.

No vaporization was observed in these simulations. The vapor pressure P_v of KCl at 1049, 1294, and 1680 K (the normal boiling temperature) is 61, 635, and 1.01×10^5 Pa, respectively.[59] The equilibrium flux of particles, n, that strike (and consequently leave) a surface is given by[60]

$$n=\alpha P_v(2\pi m k_B T)^{-1/2}\,, \tag{12}$$

where α is the fraction of particles of mass m that condense. The probability that an ion pair will leave one of the film's surfaces within 20000 time steps is 3×10^{-4}, 10^{-2}, and 0.5 at 1049, 1294, and 1680 K (assuming $\alpha=1$). Consequently it is not surprising that vaporization was not observed in these simulations.

The interfacial thickness L is a quantity frequently quoted in the literature in order to characterize an interface and is defined by[61]

$$L=\rho\left[\left.\frac{d\rho(z)}{dz}\right|_{z=z_e}\right]^{-1}\,, \tag{13}$$

where z_e is the equimolar dividing surface. For both KCl temperatures it was statistically indistinguishable from 5.5±0.5 Å. Notice that for KCl and LiCl no surface excess adsorption of one of the species was observed in Figs. 7 and 8, as has been predicted by Sluckin,[11] but see later for a further discussion of this important subject.

D. Thermodynamic profiles

Perhaps the simplest thermodynamic profile is for the temperature, $T(z)$. The $T(z)$ profiles of a selection of the films are presented in Fig. 9. Thermodynamically one expects a constant value through the film for this classical system. As far as one can discern this is obeyed. Note that the temperature fluctuations were larger at a liquid-vacuum surface than at the center of the film due to the poorer statistics associated with the comparatively smaller number of particles in the interphasial region. A finer resolution of the single-particle temperature fluctuation would perhaps reveal a surface enhancement in the specific heat. In some respects the density variation in the interphasial region masks the uniformity of thermodynamic parameters well into the interface. For example, the 1049-K KCl free film can be used to obtain the configurational energy density, $E(z)$, which is defined as

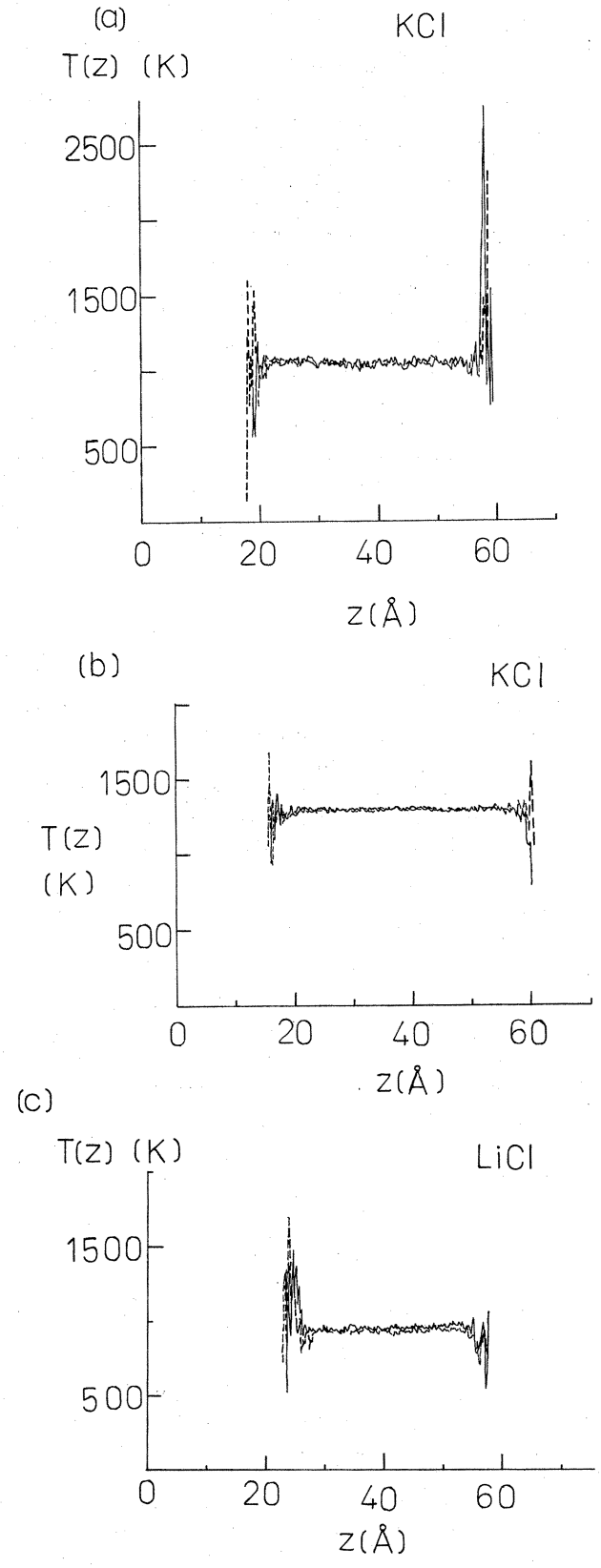

FIG. 9. Temperature profiles, $T(z)$, across the films (a) KCl: $\langle T\rangle = 1049$ K, $S = 20.22$ Å and evolved for 15 001 time steps. (b) KCl: $\langle T\rangle = 1294$ K for 20 300 time steps. (c) LiCl: $\langle T\rangle = 947$ K for 11 300 time steps.

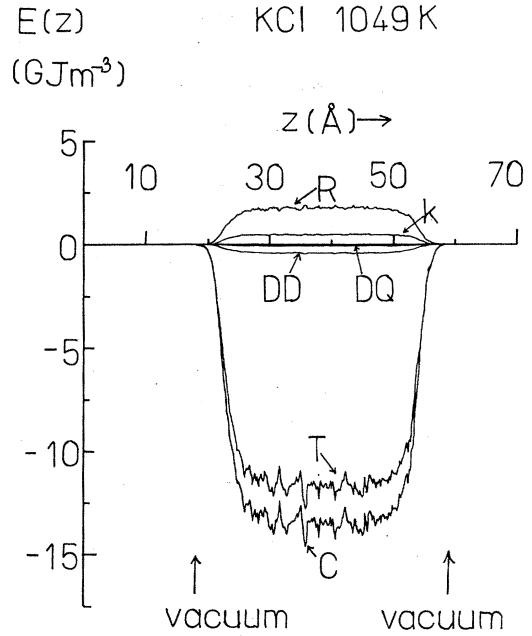

FIG. 10. Energy density profiles for the 1049 KCl free film bounded by two vacuum-model melt interphases. A resolution into the energy components is made: C, R, DD, DQ, and k denote Coulomb, short-range—repulsive, dipole-dipole, dipole-quadrupole, and kinetic components, respectively.

$$E(z)=\frac{1}{2}\frac{1}{S^2\Delta z}\sum_{i=1}^{N}\sum_{\substack{j=1\\ j\neq i}}^{N}\phi_{ij}(r)\,, \tag{14}$$

where Δz equals 0.2 Å for all profiles here. r_{zi} is within $\pm\frac{1}{2}\Delta z$ of z. Figure 10 shows a very narrow plateau region for the Coulombic component of (and hence total) $E(z)$. In comparison, the energy-per-ion profiles (i.e., $E(z)/[\rho_+(z)+\rho_-(z)]$) in Fig. 11 show much flatter and

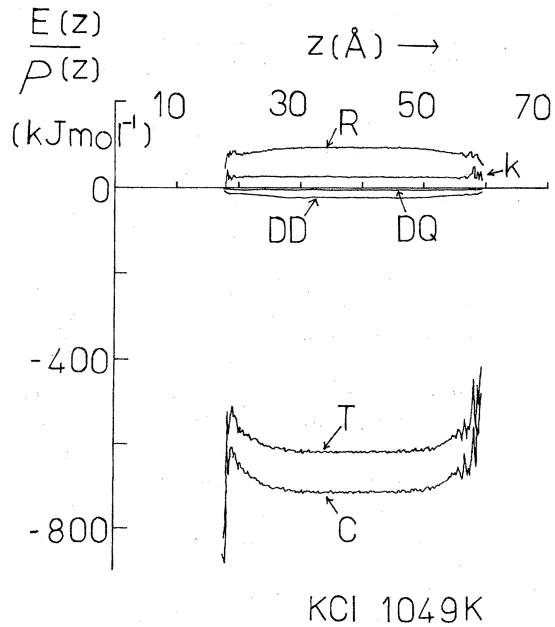

FIG. 11. As for Fig. 10 except that the energy per particle of this system is shown.

smoother profiles. Consequently each ion experiences a bulklike environment closer to the vacuum than would at first be expected from $E(z)$. When this film is confined by repulsive walls, as described elsewhere,[39] the density oscillation leads to a highly structured $E(z)$ (see Fig. 12). The structure evident there is quite markedly damped down in the corresponding energy-per-ion profiles illustrated in Fig. 13(a). In Fig. 13(b), the VACF's in the neighborhood of the walls reveal that ionic motion becomes anisotropic so that when compared with bulk behavior, oscillations are stronger perpendicular but weaker tangential to the wall planes.

These profiles raise an interesting point related to definitions of intensive and extensive thermodynamic quantities in the interphasial region. Only for certain thermodynamic functions can one predict the behavior across the interface. We have already seen that the temperature is constant in the interphasial region. The volume per particle goes from intensive to extensive in the direction of the vacuum. This impacts on the energy per particle and also on the components of the pressure tensor, which was resolved in the directions parallel and perpendicular to the surface:[62]

$$P_{\parallel}(z)=\frac{1}{2}\left[\sum_{i}^{N}\left[m_i(\dot{r}_{xi}^2+\dot{r}_{yi}^2)-\tfrac{1}{2}\sum_{j\neq i,j=1}^{N}\frac{r_{xij}^2+r_{yij}^2}{r_{ij}}\frac{\partial\phi_{ij}}{\partial r}\right]\right]\Big/\Delta z\,S^2 . \tag{15}$$

Again,

$$z-\frac{\Delta z}{2}<r_{zi}<z+\frac{\Delta z}{2} .$$

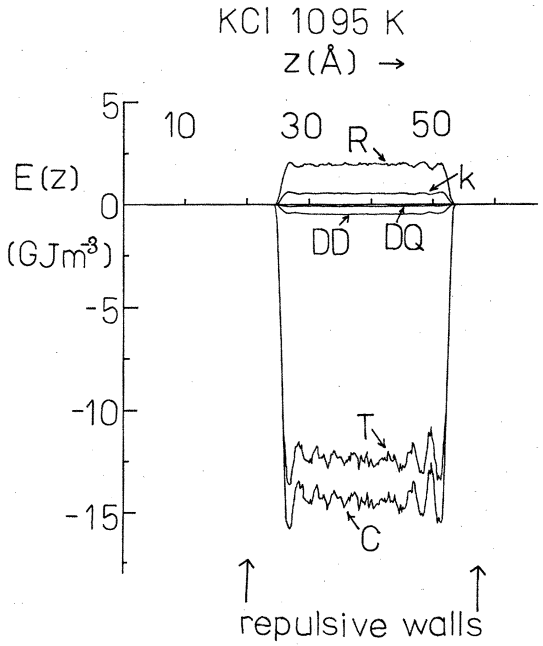

FIG. 12. Energy density profiles for the 1095 K KCl infinite film bounded by two repulsive-wall/melt interfaces. A resolution into energy components as for Fig. 10 is given. The simulation was for 21 000 time steps (or 156 ps).

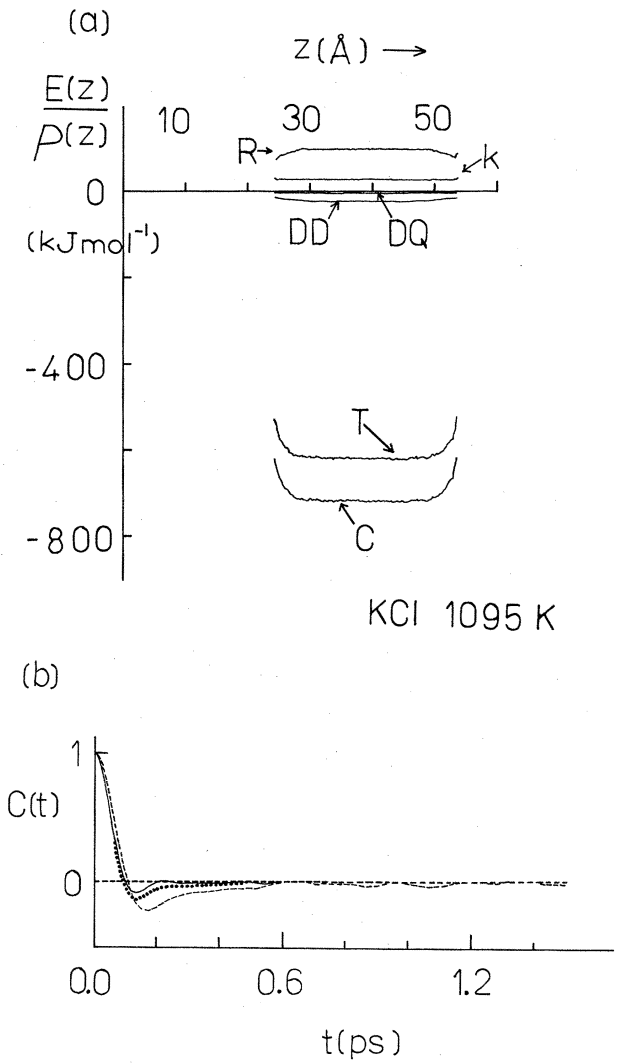

FIG. 13. (a) The energy per particle profile for the system of Fig. 12. (b) The normalized velocity autocorrelation function (VACF) for the ~6 surface K^+ in the perpendicular, — — —, and parallel, ——, directions to the interphase planes. Also shown is the K^+ VACF for the central ~35 K^+ (· · · ·).

Similarly for the perpendicular component,

$$P_{\perp}(z)=\left[\sum_{i=1}^{N}\left[m_i\dot{r}_{zi}^2-\tfrac{1}{2}\sum_{j\neq i,j=1}^{N}\frac{r_{zij}^2}{r_{ij}}\frac{\partial\phi_{ij}}{\partial r}\right]\right]\Big/\Delta z\,S^2 . \tag{16}$$

Although there is some confusion over the unique definition (if any) of the normal pressure[62] in the interfacial region, the form defined by Eq. (16) was evaluated in the simulations and shows a zero value (within statistical uncertainty) in the central region, where it should be uniquely defined. This is to be expected on the grounds of mechanical stability because the normal pressure must be zero in the z direction due to the absence of vapor. There is some departure from zero in the interphases which we ascribe to poor statistics in this region.

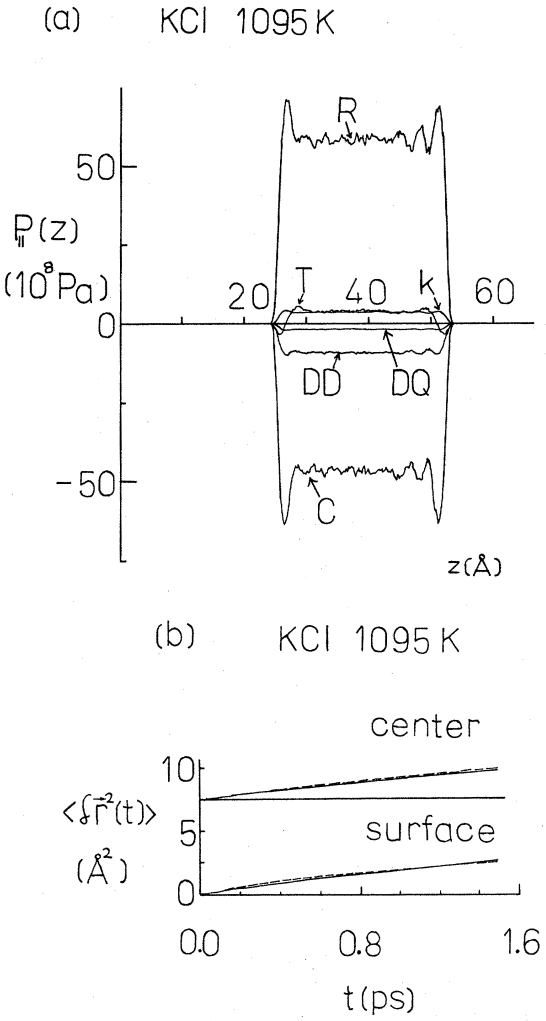

FIG. 14. (a) The component of the pressure tensor in the surface plane, $P_{\|}(z)$, as a function of z for the model KCl 1095 K film separated by two repulsive walls. (b) The Cl^- mean-square displacements parallel (——) and perpendicular (— — —) to the surface planes for this state.

E. Confined films

The $P_{\|}(z)$ for the 1095-K model KCl film confined between repulsive walls is shown in Fig. 14. The increase in ion density near the hard walls is manifest in the components of $P_{\|}(z)$ which are larger than in lower density parts of the film. There is a minimum in the total $P_{\|}(z)$ in the interphase, which gives rise to surface tension.

The mean-square displacements of ions in the interphase and center support the conclusions already derived from the VACF and pressure profiles, in reflecting perturbed dynamics at the interface. They are obtained from the appropriate mean-square displacements from an arbitrarily chosen time origin.[39] The tangential, perpendicular (to the surface planes), and bulk diffusion coefficients are for the 1095-K confined film: 0.93, 0.95, and 0.76 (K^+); 0.93, 0.91, and 0.81 (Cl^-). Figure 14(b) shows the mean-square displacements used to generate these values. Figure 15 presents some similar plots for the 1294-K free-film KCl simulations. Here the enhanced diffusion perpendicular to the surface planes and near the vacuum is more strongly apparent. Further discussion of the effect of an interphase on ionic dynamics is given in the next section.

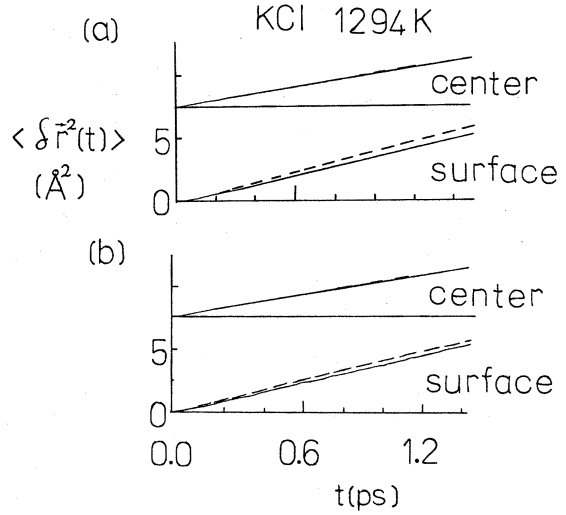

FIG. 15. The mean-square displacements of the surface 4 to 5 ions closest to the vacuum, and the central 35 ions of each ionic species. As before —— refers to tangential motion and — — — to perpendicular motion. (a) K^+ and (b) Cl^- for the 1294 K model KCl free film (i.e., with two melt-vacuum interfaces).

F. Interphasial dynamics

Molecular dynamics is well suited to the investigation of the microscopic dynamics of the system studied (this being a major advantage over the Monte Carlo method[34]). However, interphasial dynamics are difficult to characterize due to the absence of easily calculated transport coefficients in this inhomogeneous region.

Transport properties of molten salts were considered by Berne and Rice[63] to consist of hard collisions each with a large transfer of momentum arising from the interactions of the ion cores and parametrized by the short-range repulsive component of the pair potential. This is followed by many softer interactions characterized by much smaller relaxation times within the force autocorrelation function. Therefore, ion motion was considered to consist of a sequence of independent hard collisions which are decorrelated by small quasi-Brownian diffusive steps. Smedley and Woodcock[64] performed MD calculations on model liquid argon and KCl to test the validity of the assumptions in this model. They concluded that the "soft" Coulomb forces and "hard" short-range contributions to momentum-exchange decay on the same time scale. This was discovered by an extensive force (and velocity) autocorrelation function analysis. There is quite a strong coupling between the soft and hard processes (evident in the cross correlation functions) and successive "collisions" are difficult to isolate. It is possible, however, that another decomposition of the ionic potential into a better resolved

short- and long-range part would provide this separation of time scales. To perform this, the short-range potential must consist of *both* repulsive and Coulomb contributions. The long-range part would presumably consist mainly of the Coulomb component at large interionic separations.

In an interphasial region the increase in free volume destroys the on-average spherical symmetry. This introduces a long time tail in the velocity autocorrelation function as the ions couple (mainly via the Coulomb interactions) to the slow density fluctuations in the interphase. There is a preferred direction of motion (into the vapor) in the interface.[65] The equivalence between the mean-square displacements and integral under the VACF, $C(t)$, routes to the diffusion coefficient, which is applicable in the bulk, is consequently not valid here. In the bulk phase the VACF can be used to obtain the self-diffusion coefficient from the following transformation:

$$D=\frac{k_B T\pi}{m}P(0)\,, \tag{17}$$

where m is the mass of the particle, k_B is Boltzmann's constant,

$$P(\nu)=\pi^{-1}\lim_{t_c\to\infty}\int_0^{t_c} dt\, C(t)\cos(\nu t)\,, \tag{18}$$

where $P(\nu)$ is the power spectrum of the normalized [i.e., $C(0)=1$] VACF, $C(t)$, at frequency ν; t_c is the truncation time of the VACF ($=1.5$ ps here).

At 1049 K the interphasial tangential, perpendicular, and bulk K^+ diffusion coefficients are 1.1, 1.3, and 0.75×10^{-4} cm^2s^{-1}, respectively. These numbers are obtained from the slopes of the mean-square displacements, MSD, in the time region 0.3 to 0.6 ps. The integral under the VACF in contrast gives 0.9, 0.5, and 0.6×10^{-4} cm^2s^{-1}, respectively. In all the calculations, the VACF perpendicular to the walls in the surface region gives a very low diffusion coefficient (lower than in the bulk). This is not consistent with the D value actually observed from the mean-square displacements (probably a better source of D).

This observation is quite forcefully demonstrated in Fig. 16. The power spectra of some interphasial VACF for free and confined films are shown. For perpendicular motion in the interface the intercept at $\nu=0$ is often hardly distinguishable from zero. In marked contrast, the MSD always produce surface diffusion coefficients which are larger than those of the appropriate bulk system, which is a more intuitively reasonable result.

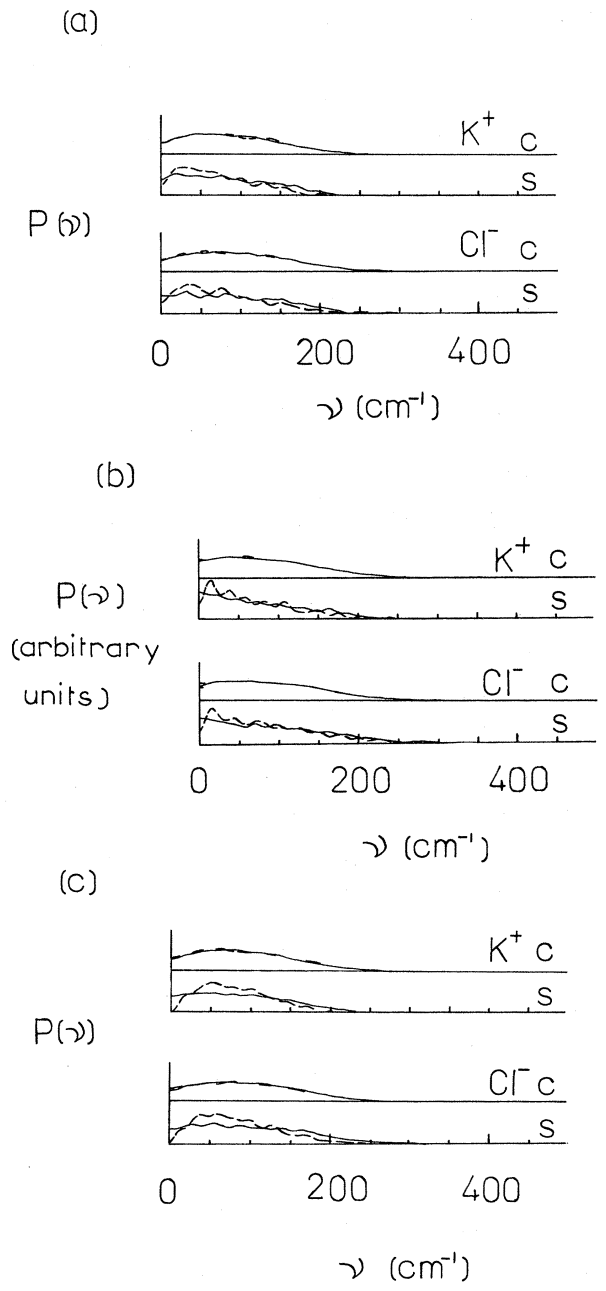

FIG. 16. Power spectra derived from the real Fourier transform of the normalized velocity autocorrelation functions for motion perpendicular (— — —) and parallel (——) to the surface planes. (a) KCl free film at 1049 K, (b) KCl free film at 1294 K, (c) KCl film between repulsive walls at 1095 K. C stands for the central ~35 ions for each species, S denotes the 4 or 5 ions closest to the wall at the beginning of the VACF time origin. The ionic species are given on each figure.

G. Charge separation in the interphase

The influence of the Coulomb term here is also strongly evident in these interfacial studies. There is a remarkable reluctance for the two species to noticeably decouple in a (100) crystal or melt surface to form a double layer, even for salts consisting of very disparate ion pairs.[66] It would be interesting to achieve such charge separation in the direction perpendicular to the surface planes. The remainder of this paper is an account of attempts to promote this; which is equivalent to the formation of a surface dipole moment.

The first system considered was a regular lamina of (111) planes such as are found in an alkali halide fcc crystal and are illustrated in Fig. 17. The MD cell contained 162 ions forming 18 (111) layers each having 9 like ions per layer within the MD cell. The x and y sidelengths were equal with a value $3a_0/\sqrt{2}$, where a_0 equals twice the nearest-neighbor distance in the crystal. The internal angles between the sides were 60°, 120°, 60°, and 120°.

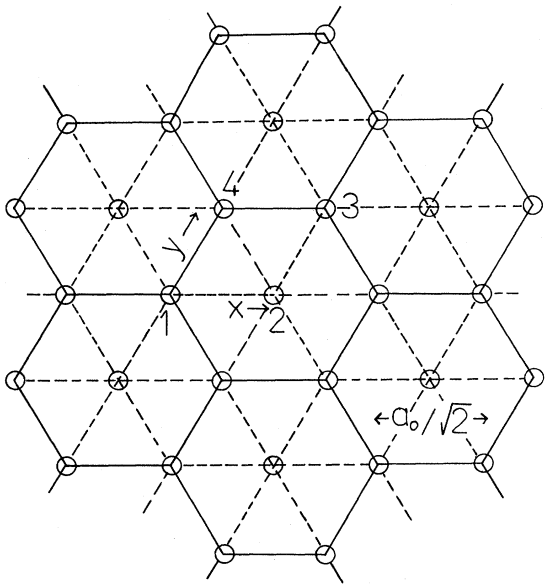

FIG. 17. A (111) plane of ion 1 and its images. This two-dimensional Bravais lattice is used to generate a lamina. Six ions in a basic unit cell are needed with projected coordinates within the parallelogram marked by 1,2,3,4 on the figure. These coordinates are $(x,y)\sqrt{2}/a_0$: (1,0), $(\frac{2}{3},\frac{2}{3})$, $(\frac{1}{3},\frac{1}{3})$, $(\frac{1}{3},\frac{1}{3})$, (1,0), and $(\frac{2}{3},\frac{2}{3})$; $z/(\sqrt{3}a_0)$: $(0,\frac{1}{3},\frac{2}{3},\frac{1}{6},\frac{1}{2},\frac{5}{6})$. The first and second sequences of three are for each ionic species.

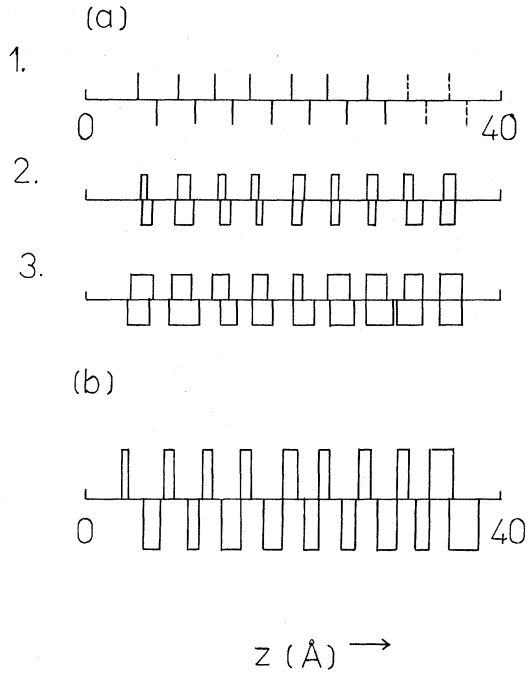

FIG. 18. (111) layer average positions and spread for the 18-layer model TF KCl state at ~200 K. The time step was 0.5×10^{-14} s. (a) Unsubstituted lamina, averages over: (1) $1<t/\Delta t\leq40$; (2) $60<t/\Delta t\leq80$; (3) $130<t/\Delta t\leq180$. (b) Lamina's surface layer of K^+ and Cl^- are substituted by 25% of the other species. This reduces the average charge per surface layer to 50% of those of the internal planes. The profile is over $80<t/\Delta t\leq120$.

Ions leaving a side reentered through the opposite side with the same side coordinates. This construction was favored to that of the more complex, but fascinating, hexagonal MD cell which was considered at first. Alternating layers were constructed solely from the same species. The dynamical evolution of this system proceeded using the method for evaluating the long-range Coulomb correction method as given by Eqs. (7) to (9). Although the symmetry of the two-dimensional sublattice is not square (and hence the dipole terms should have different coefficients[40]), test calculations on static configurations suggested that the errors are small when compared with the uncertainties in the choice of R_c. The following calculations reported were performed with this lattice-summation method.

Figure 18 shows the time development of the layer positions and approximate widths in the z direction for a (111) KCl lamina maintained close to 200 K. Within 0.9 ps the staggered layers of pure positive and negative charges in a regular lamina start to overlap and then go more diffuse afterwards. This produces a sharp rise in pressure (~30 kbars). This state requires a velocity scaling factor of ~0.93 each time step to maintain the preset temperature. Within the constraints of rhombohedral boundary conditions a path to a stable configuration was not found, and would possibly require a more generalized form of MD; an example is that developed by Parrinello and Rahman.[67] The angles between the sides (formed between the xz and yz planes) would have to change according to the demands of the internal stresses. It may also be necessary for this to be made z dependent.

Conditions for stabilizing these polar faces were established by Fripiat *et al.*[27] For a 1:1 (111) fcc face it was shown that a surface-layer charge reduction of 50% must be achieved. A MD simulation in which $\frac{1}{4}$ of the surface-layer ions were replaced by those of the other species was made, so that no replacements were next to each other. This sample showed only a slightly reduced tendency to produce overlapping layers [see Fig. 18(b)].

It is possible that a polar crystal face could achieve mechanical equilibrium because of the balance of in-built internal stresses. In contrast, a melt surface, as we have seen, does not obviously form a double layer because the ions are then mobile and seek an on-average distribution which satisfies overall neutralility in each volume element enclosing a plane parallel to the surface and a small increment of distance in the perpendicular direction. In an attempt to assess the resistance to such charge separation, a series of simulations on a 216-ion molten NaCl BMH (Tosi-Fumi) film were performed. They differ from those discussed earlier by being accompanied by an externally applied electric field in the direction perpendicular to the surfaces. The motivation for this was to discover the form charge separation takes in the melt when artificially induced by an external perturbation that discriminates between cation and anion.

First, however, an extensive calculation on a model liquid NaCl film was performed at 1195 K and a molar volume of 39.1 $\mu m^3 mol^{-1}$ (S=19.14 Å and N=216)

without an applied electric field E in the z direction (i.e., perpendicular to the surface planes). The simulation evolved for 68 ps in production. The total energy and pressure were $-674.90(\pm 0.2)$ kJ mol^{-1} and $1.34(\pm 2.14)$ kbars. The single-ion density profiles are shown in Fig. 19. No statistically significant charge separation in either interphasial region is noted, which is in good agreement with the earlier studies on molten LiCl and KCl, and at first sight contrary to the predictions of Sluckin.[11] However, the instantaneous dipole moments at a surface give values for the potential drop across the interface which are tens of volts (an order of magnitude larger than the time averages predicted by Sluckin[11]). There is an extremely slow relaxation of structure in the interphasial region which is noticeable between 10-ps subaverages and is proportional to the surface excess dipole. One would need very long simulations to obtain good statistics to be confident about the nature of the surface dipole moment perpendicular to the surfaces. It is perhaps understandable when it is realized that the potential energy between a NaCl pair at the minimum [=2.36 Å (Ref. 32)] is 6 eV. Therefore, small displacements of only one ion pair are sufficient to give a potential change across the interphase which is of the same order of magnitude that Sluckin predicts. In fact, movements of particles within the elements of the z-profile histograms, which have a width of 0.4 Å here, would almost produce these voltage changes. Consequently species differences would not even register in the profiles, as a result.

We now consider the pressure tensor component profiles in the z direction, $P_\perp(z)$. As expected $P_\perp(z)$, shown in Fig. 20(a), is zero in the center of the film because the surrounding medium is a field-free vacuum and therefore must be at zero pressure. It also has a positive peak and then a negative trough as one passes from the vacuum into the center of the film. This is difficult to explain, but must result from the balance between certain, as yet undefined, constraints. In contrast, the tangential component of the pressure tensor, $P_{||}(z)$, is positive in the center of the film, as Fig. 20(b) reveals. This indicates that the film is not isotropic in the center, which surely must derive from the long-range nature of the Coulomb forces. Note that the surface tension, as usually evaluated[62] from the difference between normal and tangential pressure tensor components, integrated across the interphase, cannot be applied here. This was discussed in some detail in a preliminary report of this work.[39] Nevertheless an approxi-

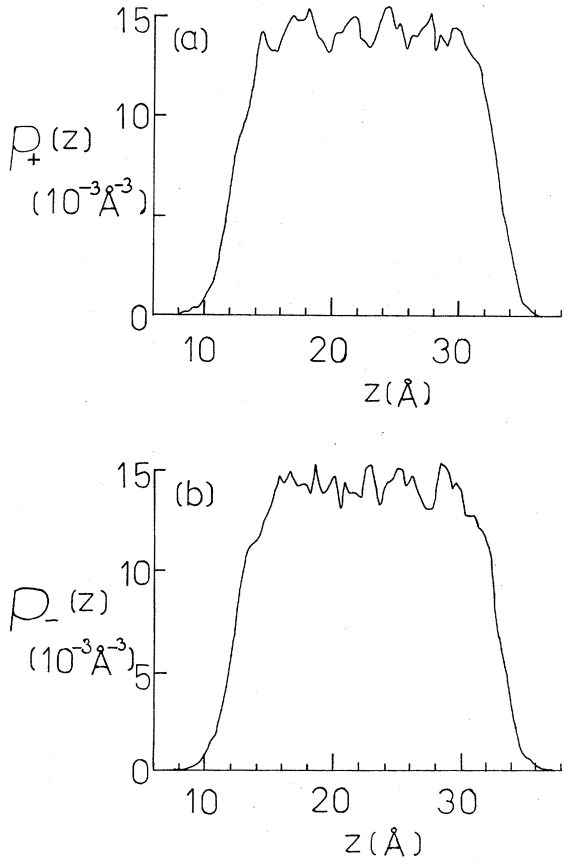

FIG. 19. Reduced number density in the z direction for a 13 500 time step (68 ps) model isolated film NaCl simulation at $\langle T\rangle = 1195.2$ K. $V_m = 39.1$ μm^3 mol^{-1} and the periodicity length equals 19.14 Å, $N=216$, histogram resolution is 0.4 Å. (a) Na^+; (b) Cl^-. No electric field is applied.

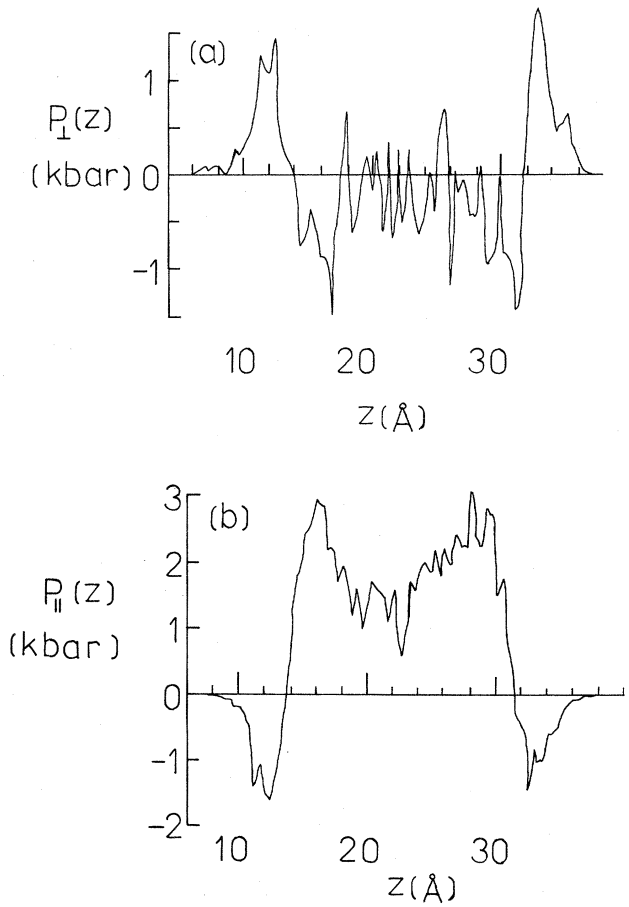

FIG. 20. Pressure tensor component profiles in the z direction for the system of Fig. 19. (a) The perpendicular (z) component $P_\perp(z)$, (b) the tangential (xy) component $P_{||}(z)$.

mate value of 0.1 $N m^{-1}$ extracted from these profiles agrees with the experimental figure.[68]

The effect of varying magnitudes of applied electric field E, in the z direction, was examined. Fields of progressively larger magnitude were applied for $\sim 10^4$ time steps (each of duration 0.5×10^{-14} s). They were 0.36, 0.72, and 1.44 $V Å^{-1}$. The lowest field of this sequence was chosen so as to be of the order of the root-mean-square force on ions in the unperturbed film. These simulations were conducted under isothermal conditions by the usual velocity scaling procedure. The scaling factor f was based on the previous time step's average temperature. However, the average value of f was found to be 1.000. The reason that no on-average cooling was necessary is that the field does not introduce a steady-state ion current in the z direction.

There is evidence that the field introduces an asymmetry on *both* species' component density profiles. There is a strong coupling between the two types of ions in the surface region. The interphase from which the Cl^- was induced to depart (i.e., the "anode") had an on-average broader tail into the vacuum than the other interface, possibly because the Cl^- have a greater inertia than the Na^+ and were therefore less easily deflected from preferentially outward trajectories. This is evident for $E=0.36$ $V Å^{-1}$, run for 50 ps, and even more so for $E=0.72$ $V Å^{-1}$, run for 40 ps, as Fig. 21 reveals. Both Na^+ and Cl^- profiles are broad, which again indicates the reluctance of the melt to charge separate and hence depart from electroneutrality tangentially in the surface planes. The trough in $P_{||}(z)$ next to the vacuum present in the equilibrium film largely disappeared for $E=0.72$ $V Å^{-1}$, as shown in Fig. 22. Hence, the surface tension is approaching zero. This destabilization of the surface becomes manifest in the density profiles for $E=1.44$ $V Å^{-1}$, run for 45 ps. Figure 23 shows an average density profile over a 10-ps time window of the simulation. It is evident that ion pairs leave one surface, whereas the next 10-ps section reveals departure of ions from the opposite surface. During the next 20 ps no ion pairs are observed to leave either surface. It appears that the dynamics must produce surface configurations which are susceptible to ion desorption by the applied field. Therefore, ion pairs leave the surface intermittently.

By positioning the NaCl film between two repulsive walls characterized by a parabolic potential and then applying an electric field between them, it was found that charge separation could be produced. The repulsive wall potential was

$$V(\delta z)=\frac{A}{4}(\delta z/Å)^2 , \tag{19}$$

where $A=2.3\times10^{-19}$ $J Å^{-1}$ and δz is the particle's displacement into the "vacuum" from a defined position in the interphase. The wall forces in the z direction were on the order of the root-mean-square force in the liquid and were the same for both species. The electric field applied was 1.44 $V Å^{-1}$. Using Gauss's law[38] then the surface charge density $\sigma(\mu C\,cm^{-2})$ is

$$\sigma=\frac{(4\pi\epsilon_0\epsilon_r)E}{4\pi}=8.85\times10^{-10}\,E(V\,m^{-1}) , \tag{20}$$

assuming that the permittivity of the melt is that of free

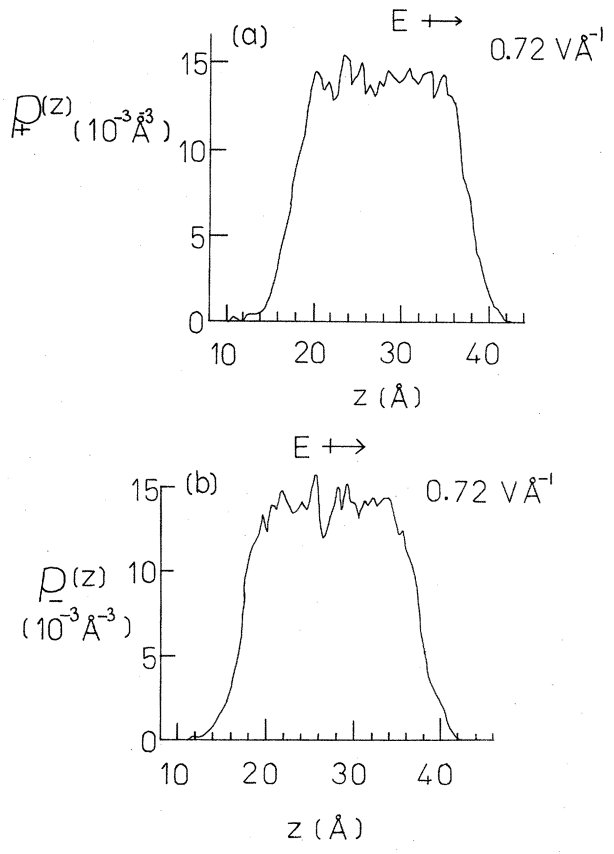

FIG. 21. Reduced number density in the z direction for a 8000—time-step ($\Delta t=0.5\times10^{-14}$ s) model NaCl isolated film simulation at $\langle T\rangle=1194.1$ K. An applied field of 0.72 $V Å^{-1}$ is applied in the z direction so as to induce the Cl^- into the left interphase. $V_m=39.1$ $\mu m^3 mol^{-1}$, $N=216$, histogram resolution is 0.5 Å. (a) Na^+, (b) Cl^-.

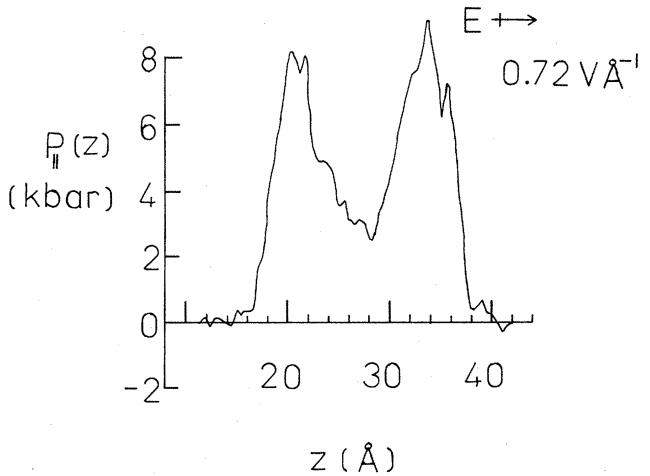

FIG. 22. The parallel component of the pressure tensor $P_{||}(z)$ in the z direction for the system of Fig. 21.

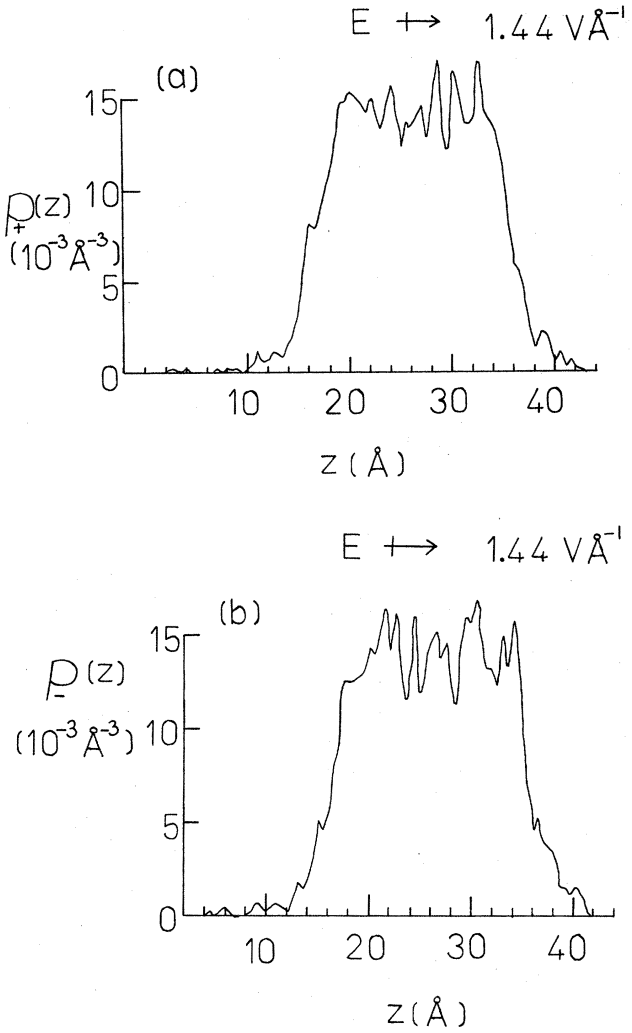

FIG. 23. The reduced number density in the z direction for a 10-ps subaverage within a model NaCl isothermal simulation at $\langle T\rangle = 1194.5$ K; $V_m = 39.1\ \mu m^3\,mol^{-1}$, $N=216$, the histogram resolution is 0.5 Å. (a) Na^+, (b) Cl^-. An applied electric field in the z direction had a magnitude of $1.44\ V\,Å^{-1}$.

space, i.e., $\epsilon_r = 1$. Now defining an excess charge density $q(z)$ to be

$$q(z) = q_+\rho_+(z) + q_-\rho_-(z)\ , \tag{21}$$

then the potential change through the interface $\phi(z)$ is given by

$$\phi(z) = \frac{-4\pi}{(4\pi\epsilon_r\epsilon_0)}\left[\int_0^z z'q(z')dz' - z\int_0^z q(z')dz'\right]. \tag{22}$$

The potential drop across the "cell" derived from Eq. (22) is 29.8 V, which within statistics is equal and opposite to the applied potential drop. The value from Eq. (22) is much larger than those obtained for comparable studies on dilute electrolytes, which were less than a volt.[3,4] The surface charge densities σ are similar to those used here, but the number density of the charged species was at least an order of magnitude smaller. Also, as $\epsilon_r \approx 20$ then the ions in the electrolyte experience a much reduced "electrode" force, resulting in a diffuse distribution of ions near each "electrode." The density usually decays monotonically from a maximum close to the wall. The melt excess charge density profile is extremely oscillatory as Fig. 24 illustrates. The corresponding $\phi(z)$ is in contrast almost linear in its decay from 0 to approximately ~ -30 V across the cell on increasing z. The potential drop across the cell, obtained from Eq. (22), is (within statistical uncertainty) equal and opposite to that of the applied field's potential change.

The effect of an electric field which is *parallel* to the interfaces of a melt-vacuum system was also investigated. A field of $0.36\ V\,Å^{-1}$ in the x direction was applied to all ions in the MD cell. No noticeable change in interfacial width was observed over 16 ps. The x velocity profile for Na^+ is shown in Fig. 25. The drift velocities in the x direction for the central plateau region are compatible with a specific conductivity of 13 mho cm^{-1} at 1229 K. This is approximately three times the value obtained by Ciccotti *et al.*[69] for a similar system by difference in trajectories MD simulation and by experiment (i.e., =4.2 mho cm^{-1}). This could be due to a nonlinear effect, expected at this large field and indeed observed by Sundheim.[70] The equivalent conductance for the bulk region of the film is 0.049 $\Omega^{-1}\,m^2\,mol^{-1}$ which is also larger than the *linear* experimental value of 0.016 $\Omega^{-1}\,m^2\,mol^{-1}$.[68] Perhaps the most fascinating feature in Fig. 25 is the *decrease* in the ionic mobility in the interphase. This is the reverse of expectations based on free-volume considerations. Note, however, that ionic forces are much stronger in the interphase than in the bulk because of reduced cancellation of the Coulomb interactions. This would imply that structural evolution in the interphase is slower than in the bulk. The ions resist imposed forces more effectively in the surface region. Both species

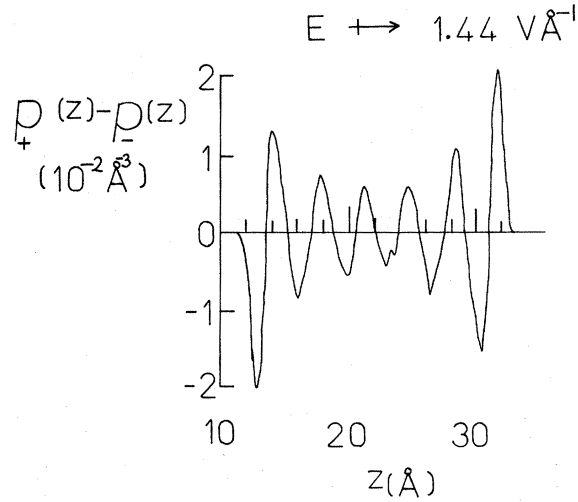

FIG. 24. The charge excess profile $\rho_+(z) - \rho_-(z)$ for a model NaCl molten film bordered by repulsive walls as given by Eq. (19). $V_m \sim 39.1\ \mu m^3\,mol^{-1}$, $N=216$, the histogram resolution is 0.4 Å. The simulation was for 25 ps. An applied electric field in the z direction had a magnitude of 1.44 $V\,Å.^{-1}$. $\langle T\rangle = 1194.1 \pm 9.5$ K.

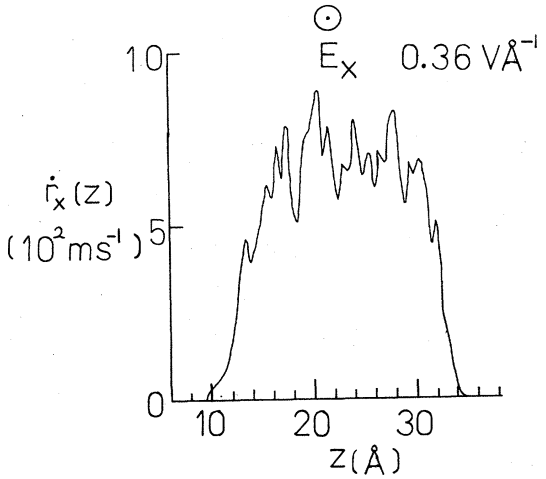

FIG. 25. The Na^+ x-velocity profile in the z direction for a $N=216$ model NaCl free-film MD simulation. An average over 3250 time steps ($\Delta t = 0.5\times10^{-14}$ s) was made. An applied field of 0.36 $V Å^{-1}$ was established in the x direction. $\langle T\rangle = 1229.4\pm11.1$ K. The melt was bounded by vacuum half spaces on either side of the film in the z direction.

exhibit this property. The associated z velocities show no consistent trend and fluctuate about zero. The x drift velocities achieved at steady state are several times larger than the equilibrium root-mean-square velocities.

III. CONCLUSIONS

It is now almost routine to simulate ionic crystal and melt interfaces. A number of isolated simulations of these systems appeared in the 1970's in this field. It is the purpose of this report to bring together a number of new insights into these systems before progress towards more complicated materials is considered.

The extent to which the Coulomb term in the pair potential has an influence on bulk and interphasial dynamics is demonstrated. On a related technical note, the Evjen method (used to determine the electrostatic potential) was discussed and refined to enable it to be practicably used (in favor of an Ewald-type expansion) in an MD surface program. A suggested corresponding-states treatment of the alkali halide system using a two-parameter pair potential was tested and shown to reproduce many of the features of a parallel calculation using the significantly more complex Born-Mayer-Huggins pair potential.

The method for achieving a crystal or melt-vacuum interface was discussed. The properties of solid and liquid thin films attached to attractive solid substrates were outlined. This approach was rejected in favor of an isolated lamina method in which a free film is positioned between two semi-infinite vacuum half spaces.

An ionic interphase near the normal melting temperature is very narrow for many properties and extends only for approximately ~15 Å into the bulk of the condensed phase. The rapid change in density and anisotropy of this region results in an ambiguity of definition for certain bulk variables when transferred into the interphasial region. The self-diffusion coefficient and the pressure are two such quantities which lack clear methods for calculation.

Attempts to observe charge separation in the surface region were unsuccessful. The (111) face of model NaCl is unstable to rearrangement of (probably) neutral planes of ions. The melt also did not manifest resolvable differences in anion (Cl^-) and cation (Na^+) density profiles in the direction perpendicular to the surface planes as a result of a 0—1.4 $V Å^{-1}$ electric field applied perpendicular to the surfaces. The surface segregation thought to exist in these melts is not discernable within the statistical fluctuations of a reasonably long simulation and will have to wait for further studies. One should conclude that the electric field produced by interphasial charge separation is destabilizing and the surface will reorganize to nullify this, unless bounded by a hard wall, when a multilayer can form on the application of an external electric field.

An interesting effect was observed when an electric field was applied in the surface plane. The ionic mobility in the interface was *less* than in the bulk. The surface tension introduces a slowly evolving interphasial structure which probably slows down motion in the tangential direction.

ACKNOWLEDGMENTS

The author is indebted to Dr. J. H. R. Clarke and Dr. L. V. Woodcock for valuable discussions. Support by the Science and Engineering Research Council of United Kingdom is gratefully acknowledged.

[1]J. S. Rowlinson, J. Chem. Soc. Faraday Trans. 2 79, 77 (1983); Chem. Br. 16, 32 (1980); J. G. Powles, R. F. Fowler, and W. A. B. Evans, Chem. Phys. Lett. 96, 289 (1983).

[2]J. A. Barker and J. R. Henderson, J. Chem. Phys. 76, 6303 (1982); P. Schofield and J. R. Henderson, Proc. R. Soc. London, Ser. A 379, 231 (1982).

[3]G. M. Torrie and J. P. Valleau, J. Chem. Phys. 73, 5807 (1981); J. Phys. Chem. 86, 3251 (1982).

[4]I. Snook and W. van Megen, J. Chem. Phys. 75, 4104 (1981); 73, 4656 (1980).

[5]S. Levine, C. W. Outhwaite, and L. B. Bhuiyan, J. Electroanal. Chem. 123, 105 (1981).

[6]D. Henderson, L. Blum, and L. B. Bhuiyan, Mol. Phys. 43, 1185 (1981).

[7]M. Lozada-Cassou, J. Chem. Phys. 75, 1412 (1981).

[8]R. Rodriguez and P. R. Antoniewicz, Chem. Phys. Lett. 66, 400 (1979); 66, 607 (1979).

[9]S. L. Carnie and D. Y. C. Chan, J. Chem. Phys. 73, 2949 (1980).

[10]R. Evans and T. J. Sluckin, Mol. Phys. 40, 413 (1980).

[11]T. J. Sluckin, J. Chem. Soc. Faraday Trans. 2 77, 575 (1981); 77, 1029 (1981).

[12]J. Goodisman, J. Chem. Phys. 73, 5844 (1981).

[13]P. V. Giaquinta and M. Parrinello, J. Chem. Phys. 78, 1946

(1983).
[14]M. Baus, Mol. Phys. 48, 347 (1983).
[15]M. Baus and C. F. Tejero, Mol. Phys. 47, 1211 (1982); M. Baus, J. Chem. Phys. 76, 2003 (1982).
[16]F. Lantelme, Mol. Phys. 47, 1277 (1982); F. Yoshida, J. Phys. C 14, 573 (1981).
[17]T. Munakata and J. Bosse, Phys. Rev. A 27, 455 (1983).
[18]S. N. Bagchi, Phys. Lett. 74A, 271 (1979).
[19]M. Rovere, R. Miero, M. Parrinello, and M. P. Tosi, Phys. Chem. Liq. 9, 11 (1979).
[20]N. H. March and M. P. Tosi, Phys. Chem. Liq. 10, 39 (1980).
[21]R. Takagi, H. Ohno, and K. Furukawa, J. Chem. Soc. Faraday Trans. 2 75, 1477 (1979).
[22]M. Dixon and M. J. Gillan, Philos. Mag. B 43, 1099 (1981).
[23]J. E. Enderby and G. W. Neilson, Adv. Phys. 29, 323 (1980).
[24]M. Feinstein, J. W. Halley, and P. Schofield, J. Phys. C 12, 4185 (1979).
[25]M. A. van Hove and P. M. Echenique, Surf. Sci. 82, L298 (1979).
[26]M. J. Yacaman, J. Phys. (Paris) Colloq. 41, C6-485 (1980).
[27]J. G. Fripiat, A. A. Lucas, J. M. André, and E. G. Derouane, Chem. Phys. 21, 101 (1977).
[28]E. Roman, G. Senatore, and M. P. Tosi, J. Phys. Chem. Solids 43, 1093 (1982).
[29]V. Massida, Physica (Utrecht) B95, 317 (1978); J. A. Hernando and V. Massida, Comp. Phys. Commun. 22, 13 (1981).
[30]R. E. Watson, J. W. Davenport, M. L. Perlman, and T. K. Sham, Phys. Rev. B 24, 1791 (1981).
[31]E. R. Smith, Proc. R. Soc. London, Ser. A 381, 241 (1982).
[32]L. V. Woodcock, J. Chem. Soc. Faraday Trans. 2 70, 1405 (1974).
[33]L. V. Woodcock, Proc. R. Soc. London, Ser. A 348, 187 (1976).
[34]D. J. Adams and I. R. McDonald, Physica (Utrecht) B79, 159 (1975); J. Phys. C 7, 2761 (1974).
[35]M. J. Gillan, Phys. Chem. Liq. 8, 121 (1978).
[36]Y. Abe and A. Nagashima, J. Chem. Phys. 75, 3977 (1981).
[37]M. P. Tosi and F. G. Fumi, J. Phys. Chem. Solids 25, 45 (1964).
[38]D. M. Heyes, M. Barber, and J. H. R. Clarke, J. Chem. Soc. Faraday Trans. 2 73, 1485, (1977).
[39]D. M. Heyes and J. H. R. Clarke, J. Chem. Soc. Faraday Trans. 2 75, 1240 (1979); 77, 1089 (1981).
[40]D. M. Heyes, Surf. Sci. 110, L619 (1981).
[41]J. S. R. Chisholm and R. M. Morris, *Mathematical Methods in Physics* (North-Holland, Amsterdam, 1966).
[42]E. A. Kraut, T. Wolfram, and W. Hall, Phys. Rev. B 6, 1499 (1972).
[43]P. P. Ewald and H. Juretschke, in *Structure and Properties of Solid Surfaces,* edited by R. Gomer and C. S. Smith (University of Chicago Press, Chicago, 1953).
[44]C. Thibaudier, J. Phys. (Paris) 30, 355 (1969).
[45]E. F. Bertaut, J. Phys. Radium 13, 499 (1952); 13, 633 (1952).
[46]L. V. Woodcock and K. Singer, Trans. Faraday Soc. 67, 12 (1971).
[47]M. Indere and K. L. Jungst, Phys. (Utrecht) 68, 180 (1973).
[48]M. T. Hutchings, Solid State Phys. 16, 227 (1964). The symmetry-adapted tesseral harmonics were obtained using a group-theory computer program written in FORTRAN by T. D. Bouman and G. L. Goodman, Chemistry Division, Argonne National Laboratory.
[49]A. D. Buckingham, Q. Rev. (London) 13, 183 (1959).
[50]D. M. Heyes and F. van Swol, J. Chem. Phys. 75, 5051 (1981).
[51]D. M. Heyes, J. Chem. Phys. 74, 1924 (1981).
[52]N. Anastasiou and D. Fincham, Comp. Phys. Commun. 25, 159 (1982).
[53]J. Michielsen, P. Woerlee, F. v.d. Graaf, and J. A. A. Ketelaar, J. Chem. Soc. Faraday Trans. 2 71, 1730 (1975).
[54]L. V. Woodcock, Proc. R. Soc. London, Ser. A 328, 83 (1972).
[55]J. W. E. Lewis, K. Singer, and L. V. Woodcock, J. Chem. Soc. Faraday Trans. 2 71, 301 (1975).
[56]S. Miller and J. H. R. Clarke, J. Chem. Soc. Faraday Trans. 2 74, 160 (1978); D. J. Adams, Chem. Phys. Lett. 62, 329 (1979); Nat. Res. Counc. Can. Proc. 9, 13 (1980); J. Chem. Phys. 78, 2585 (1983).
[57]B. W. Hatt and D. H. Kerridge, Chem. Br. 15, 78 (1979).
[58]M. Rao and D. Levesque, J. Chem. Phys. 65, 3233 (1976); F. F. Abraham, D. E. Schneider, and J. A. Barker, J. Chem. Phys. 62, 1958 (1975).
[59]*Handbook of Chemistry and Physics,* 51st ed., edited by R. C. Weast (Chemical Rubber, Ohio, 1970).
[60]J. M. Blakely, *Introduction to the Properties of Crystal Surfaces* (Pergamon, New York, 1973).
[61]S. Toxvaerd, in *Statistical Mechanics,* edited by K. Singer (Chem. Soc. Spec. Rep., London, 1976), Vol. 2; p. 256.
[62]H. T. Davis and L. E. Scriven, *Advances in Chemical Physics* (Wiley, New York, 1982) Vol. 49, p. 357.
[63]B. Berne and S. A. Rice, J. Chem. Phys. 40, 1347 (1964).
[64]S. I. Smedley and L. V. Woodcock, J. Chem. Soc. Faraday Trans. 2 70, 955 (1974).
[65]G. W. Mulholland, J. Chem. Phys. 64, 862 (1976).
[66]D. M. Heyes, M. Barber, and J. H. R. Clarke, J. Chem. Soc. Faraday Trans. 2 75, 1469 (1979).
[67]M. Parrinello and A. Rahman, J. Chem. Phys. 76, 2662 (1982).
[68]G. J. Janz, *Molten Salts Handbook* (Academic, New York, 1967).
[69]G. Ciccotti, G. Jacucci, and I. R. McDonald, Phys. Rev. A 13, 426 (1976).
[70]B. R. Sundheim, Chem. Phys. Lett. 60, 427 (1979).